biblio.ugent.be

The UGent Institutional Repository is the electronic archiving and dissemination platform for all UGent research publications. Ghent University has implemented a mandate stipulating that all academic publications of UGent researchers should be deposited and archived in this repository. Except for items where current copyright restrictions apply, these papers are available in Open Access.

This item is the archived peer-reviewed author-version of: Intracellular delivery of nanomaterials: how to catch endosomal escape in the act

Authors: Martens T., Remaut K., Demeester J., De Smedt S., Braeckmans K.

In: Nano Today, 9(3), 344-364 (2014)

Optional: link to the article

To refer to or to cite this work, please use the citation to the published version:

Authors (year). Title. *journal Volume(Issue)* page-page. Doi 10.1016/j.nantod.2014.04.011

INTRACELLULAR DELIVERY OF NANOMATERIALS: HOW TO CATCH ENDOSOMAL ESCAPE IN THE ACT

Thomas F. Martens [1,2,+], Katrien Remaut [1], Jo Demeester [1], Stefaan C. De Smedt [1,*], Kevin Braeckmans [1,2]

[1] Laboratory for general biochemistry and physical pharmacy, Faculty of Pharmaceutical Sciences, Ghent University, Harelbekestraat 72, 9000 Ghent, Belgium

[2] Center for Nano-and Biophotonics (NB-Photonics), Ghent University, Harelbekestraat 72, 9000 Ghent, Belgium

+ Corresponding author during submission: Laboratory for general biochemistry and physical pharmacy, Faculty of Pharmaceutical Sciences, Ghent University, Harelbekestraat 72, B-9000 Ghent, Belgium
Tel: +32 9264 8049
Fax: +32 9264 8189
E-mail: Thomas.Martens@Ugent.be

* Corresponding author after submission: Laboratory for general biochemistry and physical pharmacy, Faculty of Pharmaceutical Sciences, Ghent University, Harelbekestraat 72, B-9000 Ghent, Belgium
Tel: +32 9264 8076
Fax: +32 9264 8189
E-mail: Stefaan.Desmedt@Ugent.be

Abstract: Successful cytosolic delivery of nanomaterials is becoming more and more important, given the increase in intracellular applications of quantum dots, gold nanoparticles, liposomal drug formulations and polymeric gene delivery vectors. Most nanomaterials are taken up by the cell via endocytosis, yet endosomal escape has long been recognized as a major bottleneck in cytosolic delivery. Although it is essential to detect and reliably quantify endosomal escape, no consensus has been reached so far on the methods to do so. This review will summarize and discuss for the first time the different assays used to investigate this elusive step to date.

Keywords: endosomal escape, nanomaterials, intracellular delivery, assays, fusion, proton sponge, pore formation

1. Introduction

Cytosolic delivery of nanomaterials has gained a lot of interest. Recent developments in nanoscience and nanotechnology have created a library of nanomaterials with potential applications in the visualization of subcellular structures and dynamics, intracellular delivery of therapeutics, gene therapy and the treatment or diagnostics of organelle-specific diseases [1-4]. Importantly, efficient delivery to the intracellular environment is necessary for exerting their intended function. Though physical techniques are sometimes used to force the nanoparticles across the plasma membrane (microinjection, electroporation, …) [4], uptake of foreign nanomaterials usually relies on the cell's innate endocytic uptake mechanism. This results in the cargo residing in endosomes (Figure 1), thus being physically separated from the cytosol by the endosomal limiting membrane [5, 6]. Furthermore, maturation of most types of endosomes to multivesicular late endosomes is coupled with a decrease in intravesicular pH and fusion with lysosomes, potentially resulting in destruction of the functional nanomaterials by degradative lysosomal enzymes [7]. This endolysosomal sequestration and hydrolytic degradation of the nanoparticulate cargo implies that they should escape from the endosomes in a timely manner to exert or preserve their intended function.

For instance, semiconductor nanocrystals, or quantum dots (Qdots), are being explored to be used for labeling intracellular structures and molecules both *in vitro* and *in vivo* [8-10]. Not only does sequestration prevent their access to the cytosol, it also results in toxicity as a result from ion leaching by degradation in the endolysosomal environment, especially in the case of Cd^{2+}-containing Qdots [11]. For cellular labeling and *in vivo* cell tracking, MRI contrast agents can be delivered to the cell interior in the form of paramagnetic Gadolinium-nanoparticles (Gd^{3+}) [12] or superparamagnetic iron oxide (SPIO) nanoparticles [13, 14]. It has been shown that sequestration of such contrast agents in intracellular vesicles could result in quenching of the MRI signal [12, 13]. Therefore, it is often strongly preferred that

Gewijzigde veldcode
Gewijzigde veldcode
Gewijzigde veldcode
Gewijzigde veldcode
Gewijzigde veldcode
Gewijzigde veldcode
Gewijzigde veldcode
Gewijzigde veldcode
Gewijzigde veldcode
Gewijzigde veldcode
Gewijzigde veldcode

nanoparticles for imaging applications should escape from the endolysosomal pathway to the intracellular environment [12].

Intracellular drug delivery, for instance adaptive immunotherapy and gene therapy, is made possible by packaging therapeutic (macro)molecules in nanomedicine particles such as polymer micelles or dendrimers, nanogels, liposomes, mesoporous silica particles etc., that should provide protection to and mediate intracellular delivery of these therapeutics [2, 15, 16]. However, therapeutic nucleic acids exert their effect in the cytosol or nucleus of the cell. MHC-I dependent antigen presentation to CD8+ T-cells also relies on antigenic protein or peptide delivery to the cytosol of antigen presenting cells (APCs) such as dendritic cells or macrophages [17]. Endolysosomal sequestration and hydrolytic degradation drastically decreases the efficiency of drug delivery systems and should be countered by efficient endosomal escape of the therapeutic cargo to the cytosol.

A wide variety of approaches have been developed to facilitate release of nanoparticles and molecules from endosomes before lysosomal degradation, such as fusogenic peptides and photochemical internalization (PCI), which have been the topic of numerous reviews [1, 2, 4, 6, 8, 16, 18, 19]. Despite decades of research, however, endosomal escape is still recognized as a very inefficient process and a major bottleneck in cytosolic delivery of nanomaterials [2, 16, 18]. In order to improve on those methods, it is quite essential being able to detect and reliably quantify endosomal escape [18, 20]. Although different assays have been proposed to date, there is no consensus yet on how to evaluate this critical step in the intracellular delivery process.

In this review, we aim to provide an exhaustive overview of methodologies used to evaluate endosomal escape, and to discuss the usefulness and limitations of each. First, a brief overview is presented of the different mechanisms and compounds to enhance endosomal

Gewijzigde veldcode

escape. Next, an overview of reported endosomal escape assays is given, with exemplary applications and discussion on the underlying assumptions and limitations inherent to each technique. Specifically, a distinction is made between assays investigating the mechanism of endosomal escape (relating to membrane fusion or membrane integrity), and those that aim to visualize or quantify cargo release in the cytosol, regardless of the mechanism of endosomal escape.

2. Enhancing endosomal escape

Most manmade materials to enhance endosomal escape have been inspired by viral and bacterial infection pathways in the cell, which rely on endocytosis followed by cleverly evolved ways of escaping towards the cytosolic compartment [21, 22]. Typically, the endosomal membrane is initially destabilized, after which endosomal escape can occur through either pore formation, rupture or membrane fusion, depending on the nanoparticle's characteristics (Figure 2). We will briefly discuss these endosomal escape mechanisms, though the reader is referred to several recent reviews on this topic for a more detailed overview [1, 2, 4, 18].

Gewijzigde veldcode
Gewijzigde veldcode
Gewijzigde veldcode
Gewijzigde veldcode
Gewijzigde veldcode
Gewijzigde veldcode

2.1. Endosomal destabilization and pore formation

Endosomal escape is characterized by an initial membrane destabilization (Figure 2B), which is confined to the endosomes as a result of the inherent acidification during endosomal maturation (Figure 2A). The most frequently proposed mechanisms for causing endosomal membrane destabilization, cationic charge and membrane-destabilizing peptides, are discussed below. Furthermore, persistent membrane destabilization can lead to pore formation in the endosomal membrane, resulting in leakage of molecules and smaller particles from the endosomal compartment to the cytosol (Figure 2C).

Since the outer layers of endosomal membranes are typically thought to be composed of phospholipids with an overall negative charge, the interaction of endosomally trapped cationic nanoparticles with the endosomal membrane is thought to induce a "flip-flop" mechanism, where anionic phospholipids from the cytosolic leaflet will flip to the intraluminal side of the endosome [23-25]. This charge-neutralized ion pair will result in non-lamellar phase changes and subsequent membrane destabilization [25]. A permanent cationic charge can result from quaternary amine groups, as is the case with cationic lipids such as N[1-(2,3-dioleyloxy)propyl]-N,N,N-trimethylammonium chloride (DOTMA) or 1,2-dioleyl-3-trimethylammonium-propane (DOTAP). Alternatively, protonable amine groups on the nanoparticle surface can also provide a cationic charge, i.e. for materials such as poly(ethylene imine) (PEI), poly(L-lysine) (PLL) and chitosan. Importantly, since the cationic charge can sometimes be enhanced along with the acidification of the endosomal compartment, membrane destabilization will then primarily occur in acidic endosomes.

Membrane-destabilizing peptides, inspired by natural viral entry peptides such as the HA-2 subunit of the influenza virus hemagglutinin, are usually called fusogenic peptides since their conformational change exposes hydrophobic (α-helical) domains, allowing them to interact with the lipid membrane of the endosome. They can typically be divided in three different classes based on the amino acid residues present in the peptide and a slightly different mechanism of action [21, 26]: 1. anionic amphiphilic peptides, such as INF7 and E5WYG, which contain glutamate residues and undergo a conformational change from a random coil to an alpha-helix under acidic conditions (pH 5 – 5,5); 2. histidine rich peptides such as H5WYG that protonate under mildly acidic conditions and destabilize membranes due to cationic interactions and an osmotic buffering effect (also see §2.2); 3. cationic amphiphilic peptides with lysine amino acids, such as K5 and KALA that can bind anionic nucleic acids and induce a pH-independent membrane destabilization by cationic interactions with the endosomal

Gewijzigde veldcode

Gewijzigde veldcode

Gewijzigde veldcode

Gewijzigde veldcode

membrane. GALA is also widely known and contains both glutamate residues for pH dependence and histidine amino acids for cationic charge and buffering [27]. A different approach to achieve membrane destabilization, without relying on acidification, entails the interaction of the endosomal membrane with the lysogenic peptide L-leucyl-L-leucine methyl ester (Leu-Leu-OMe). This dipeptide is converted into a membrane-lysing compound, not by an acidic environment, but by the lysosomal enzyme dipeptidyl peptidase I [25, 28].

Gewijzigde veldcode
Gewijzigde veldcode
Gewijzigde veldcode

2.2. Endosomal rupture

Whereas persistent membrane destabilization can result in gradual leakage of small nanomaterials through pore formation, bursting of endosomes has also been proposed as a mechanism for endosomal escape (Figure 2D). Likely the best-known mechanism to enhance endosomal escape is the "proton sponge effect" [29], which is based on cationic polymers or lipids with excess uncharged protonable amine groups that can buffer endosomal acidification by absorbing protons in the endolysosomal compartment. As long as ATP is present in the cytosol, V-type ATPases will keep pumping protons against their electrochemical gradient across the endolysosomal membrane, with an associated influx of counter-ions to balance the transmembrane voltage difference (Figure 2A) [7, 30]. Endolysosomal rupture is currently believed to result from a combination of three effects (Figure 2D). First, the buffering compounds will induce an initial membrane destabilization by the flip-flop effect induced by the cationic charge of the protonated amine groups. Second, electrostatic repulsion of the protonated amine groups results in swelling of the buffering agent, also referred to as the "umbrella effect" [16], further contributing to membrane destabilization [10]. Third, the constant influx of counter-ions to balance the electric potential creates an osmotic gradient between vesicle and cytosol, leading to an influx of H_2O to restore the osmotic balance. With an already destabilized endolysosomal membrane, the swelling of the intracellular vesicles results in bursting of the endosome and release of the cargo in the cytosol. Typical examples

Gewijzigde veldcode
Gewijzigde veldcode
Gewijzigde veldcode
Gewijzigde veldcode
Gewijzigde veldcode
Gewijzigde veldcode

of proton sponge compounds are PEI [31], poly-amido amines [32] and imidazole-containing polymers (e.g. histidine) [2, 18]. They are typically incorporated into the nanoparticles as the delivery vector, although in some cases the buffering compounds are either co-incubated with the nanoparticles (e.g. monensin) or added afterwards (e.g. chloroquine). Similar to chloroquine, ammonium chloride and methyl-amine are lipophilic in the unprotonated form and will penetrate cellular and vesicular membranes. Upon protonation in acidifying endosomes, these compounds become trapped and can act as proton sponges [18].

In contrast to membrane destabilization triggered by the endolysosomal compartment only, certain physical techniques allow (spatio)-temporally controlled disruption of intracellular vesicles. A well-known strategy to induce rupture without the need for acidification is PCI [33, 34], which involves the use of amphiphilic photosensitizers, e.g. ethyl eosin [35] or TPPS2a (mesotetraphenylporphine carrying two sulfonate groups on adjacent phenyl rings) [33]. After pulse-chased administration of the photosensitizer to the cells *in vitro*, they will accumulate in intracellular membranes, amongst which the endosomal membranes. Upon illumination with a specific light source, excitation of the photosensitizers induces the formation of reactive oxygen species (ROS), primarily singlet oxygen. Due to a short lifetime, the damage caused by this highly reactive intermediate will be mainly confined to the proximate membranes [33]. Light has also been used as a trigger for heat-induced endosomal destabilization or rupture, for example by NIR irradiation of reduced graphene oxide [36] or by the generation of vapor nanobubbles through pulsed-laser irradiation of gold nanoparticles [37]. An alternative method to induce bursting of the endosomal vesicles in a temporally controlled manner is the so-called “osmolytic shock”. This is attained by loading the intracellular vesicles with a hypertonic solution via endocytosis and afterwards incubating the cells with a hypotonic solution, causing the intracellular vesicles to swell and burst [28, 38, 39]. Similarly, carrier materials have been developed which exhibit swelling upon a decrease

Gewijzigde veldcode
Gewijzigde veldcode
Gewijzigde veldcode
Gewijzigde veldcode
Gewijzigde veldcode
Gewijzigde veldcode
Gewijzigde veldcode
Gewijzigde veldcode
Gewijzigde veldcode
Gewijzigde veldcode
Gewijzigde veldcode
Gewijzigde veldcode
Gewijzigde veldcode

in temperature [40, 41], thereby disrupting intracellular vesicles containing the particles after a "cold shock" treatment.

Gewijzigde veldcode

Gewijzigde veldcode

2.3. Endosomal membrane fusion

Fusion of a nanocarrier with the endosomal membrane can result in escape of the nanocarrier's cargo into the cytosol (Figure 2E). Endosomal escape through fusion only occurs when the nanoparticle itself is enveloped by a membrane. It is beneficial if the endosomal membrane is already destabilized. This is the case for cationic liposomes, whose charge ensures close interaction with and destabilization of the endosomal membrane, resulting in fusion and release of the encapsulated cargo. Incorporation of fusogenic "helper" lipids (e.g. 1,2-dioleoyl-sn-glycerol-3-phosphatidylethanolamine or DOPE) further enhances endosomal fusion and escape, by undergoing a conformational change upon acidification and promoting a non-lamellar lipid phase change [42]. Cholesterol has also been integrated in liposomal particles to enhance fusogenicity in a pH-independent way, both at the plasma membrane and after endocytosis [43].

Gewijzigde veldcode

Gewijzigde veldcode

3. Studying endosomal escape mechanisms

As previously highlighted, endosomal escape involves an initial membrane destabilization, followed by pore formation, endosomal rupture or membrane fusion. Typically, the mechanisms for endosomal escape are assayed by investigating the integrity of the endosomal membrane. Though these assays can be performed in cells, a more controlled environment can be created *ex cellulo* by using artificial endosomes. These artificial endosomes are frequently modeled by creating liposomes with membranes of a known phospholipid composition, which then interact with the compound under investigation.

3.1. Verifying pH-induced membrane destabilization

The initial membrane destabilization of endosomal escape is usually triggered by an acidic pH, leading to conformational changes of fusogenic compounds or a flip-flop effect by cationic particles. The effect of pH on this membrane destabilization is investigated by comparing endosomal escape scenarios where pH either does or doesn't affect the cationic or fusogenic compounds. The difference in endosomal escape between the normal and the pH-irrelevant scenario is then evaluated using the different endosomal escape assays which will be discussed further, and have been summarized in Figure 1. Removing the influence of pH on endosomal escape is done by either altering the compound under investigation so it is no longer pH-reactive [44], or the pH of the endosomal compartment itself is altered. In a controlled *ex cellulo* environment, the pH can be modeled by using buffers with different pH [45, 46]. In cellular assays, acidification can be blocked by the use of inhibitors. Several studies report the inhibition of endosomal acidification by using a higher buffering capacity in the extracellular medium [47] or co-incubation with buffering agent such as ammonium chloride [48, 49], chloroquine [50] and monensin [48]. However, it is important to take into account that these buffering agents might enhance endosomal escape due to the proton-sponge effect, rather than block it through inhibiting acidification. Therefore, it would make more sense to block the acidification process altogether, which is done by the addition of ion channel inhibitors (ionophores) [51] or more importantly, V-type proton-pumping ATPase inhibitors such as bafilomycins or concanamycins [52].

Gewijzigde veldcode
Gewijzigde veldcode
Gewijzigde veldcode
Gewijzigde veldcode
Gewijzigde veldcode
Gewijzigde veldcode
Gewijzigde veldcode
Gewijzigde veldcode

3.2. Assays for studying pore formation

Pore formation can be investigated by measuring the leakage of tracer compounds into the extravesicular environment (see Table 1). Typically, though not always, these tracers are fluorescent molecules that are quenched inside the vesicles and become (more) fluorescent upon their escape. This increase in fluorescence intensity can be measured with

spectrofluorimetry in *ex cellulo* assays, or with fluorescence microscopy or flow cytometry in cellular assays. Flow cytometry is convenient in that it can provide a high-throughput quantification of the fluorescence intensity per cell. Fluorescence microscopy has lower throughput but has the advantage of providing additional information on the intracellular fluorescence profile (IFP). A punctate fluorescence pattern is often considered an indication of the tracer compound being entrapped in endosomes, while a diffuse cytosolic staining implies leakage from the endosomal vesicles (Figure 3). It must be noted however, that such a tracer leakage assay cannot distinguish between endosomal escape by pore formation, or by bursting (see §3.3).

8-Aminonaphthalene-1,3,6-Trisulfonic Acid (ANTS) and 8-Hydroxypyrene-1,3,6-Trisulfonic Acid (HPTS) are polyanionic fluorescent molecules that are quenched by the cationic quencher *p*-Xylene-Bis-Pyridinium Bromide (DPX). Both ANTS/DPX [55] and HPTS/DPX [55, 56] have been used in *ex cellulo* assays to investigate the membrane integrity of artificial endosomes, where leakage and dilution of both compounds results in dequenching of the fluorescent signal. Fluorescein-labeled cell-penetrating peptides (CPPs) have been used in a similar manner with potassium iodide as quencher [57]. Otherwise, rather than using a quencher molecule, self-quenching of certain fluorophores can be achieved when used at a sufficiently high concentration, which is relieved upon leakage resulting in increased fluorescence. For instance, calcein [58, 59], carboxyfluorescein (CF) [45] and sulforhodamine B (SulfoB) [61] have been used in *ex cellulo* leakage assays to investigate membrane integrity of artificial endosomes by spectrofluorimetry. In cellular assays, these tracer molecules are loaded in the endosomes by constitutive endocytosis. Especially calcein has been used for this, since the acidic pH in endolysosomes will further quench its fluorescence so that the increase in fluorescence intensity after leakage is even more pronounced. Scoring pore

Gewijzigde veldcode
Gewijzigde veldcode
Gewijzigde veldcode
Gewijzigde veldcode
Gewijzigde veldcode
Gewijzigde veldcode
Gewijzigde veldcode

formation in cellular assays using calcein has been achieved both by microscopy [47, 60] and flow cytometry [53].

Whereas an increased calcein fluorescence does not disclose from which intracellular vesicle leakage occurred, the use of other tracer molecules such as DQ-ovalbumin [38] and acridine orange (AO) [38, 47, 51] relate specifically to endolysosomal membrane integrity. DQ-ovalbumin is a 45 kDa protein to which a high number of BODIPY-FL (8-chloromethyl-4,4-difluoro-1,3,5,7-tetramethyl-4-bora-3a,4a-diaza-sindacene) is conjugated, quenching its fluorescence. Before this protein is proteolytically processed into peptides in the endolysosomal compartment, pore formation will lead to release of the quenched DQ-ovalbumin protein. However, after proteolytical degradation, pore formation will lead to release and dilution of the quenched BODIPY-FL-labeled peptides and an increase in fluorescence.

Another interesting approach to specifically investigate lysosomal integrity that doesn't involve a dequenching of highly concentrated dye, relies on acidotropic dyes like AO that accumulate at a high concentration in the lysosomal lumen, forming fluorescent dimers in acidic environments. Upon lysosomal membrane damage its fluorescence decreases because the lysosomal acidic pH can no longer be maintained in combination with AO leaking out in the cytosol. Quantification of this decreased fluorescence is then related to damage to the lysosomal membrane [38, 47, 51].

Endosomal membrane integrity can also be evaluated in cells without the use of fluorescent tracers. For instance, the leakage of certain toxins from endosomes is known to inhibit protein synthesis. In such a way, Pseudomonas exotoxin [62], ribotoxin α-sarcin [63] and saporin [64] were used as tracer molecules to investigate membrane destabilization by different viruses. The influence on protein synthesis was evaluated either with radio-actively labeled [^{3}H]-

Gewijzigde veldcode
Gewijzigde veldcode
Gewijzigde veldcode
Gewijzigde veldcode
Gewijzigde veldcode
Gewijzigde veldcode
Gewijzigde veldcode
Gewijzigde veldcode
Gewijzigde veldcode
Gewijzigde veldcode
Gewijzigde veldcode
Gewijzigde veldcode

leucine [62] or [^{35}S]-methionine [63], or by using an MTT assay [64]. Though these assays were used in a viral setting, they could easily be applied for manmade materials as well.

As already highlighted, the leakage assay is frequently used to evaluate the effectiveness of certain compounds to induce pore formation, such as viral nanoparticles [61-64] and CPPs [53, 55, 57-59]. Nonetheless, these assays were also used to verify the effectiveness of polymeric gene delivery complexes, composed of cationic polymers such as PEI [51, 60] or poly(2-alkylacrylic acid) [47], and pDNA. A limitation of detecting leakage of small molecules, however, is that it may not directly relate to the release of larger macromolecules or nanoparticles. Therefore, radioactive labeled proteins were used instead of small molecule tracers in an *ex cellulo* assay, where the radioactivity of leaked proteins in the extravesicular environment was visualized after agarose gel electrophoresis [58]. Fluorescent dextrans of various molecular weights are interesting for use in cellular assays as well since they are efficiently taken up by cells without spontaneous leakage from the endocytic vesicles, and they can be labeled with different fluorophores [38, 53, 65]. However, as leakage of dextrans into the cytosol will not lead to fluorescence dequenching, it requires visualization of the IFP with fluorescence microscopy. Of course, to distinguish punctate from diffuse staining, it is essential that these large tracer compounds are still able to diffuse throughout the cytosol, which can be checked e.g. by microinjection.

Gewijzigde veldcode
Gewijzigde veldcode
Gewijzigde veldcode
Gewijzigde veldcode
Gewijzigde veldcode
Gewijzigde veldcode
Gewijzigde veldcode
Gewijzigde veldcode
Gewijzigde veldcode
Gewijzigde veldcode
Gewijzigde veldcode
Gewijzigde veldcode
Gewijzigde veldcode

3.3. Assays for studying membrane rupture

Aside from pore formation, endosomal escape can also occur through the rupture or bursting of the endosomal vesicles when an already destabilized membrane is perturbed by an outward force, e.g. osmotic pressure (see § 2.2). The leakage assays discussed in §3.2 can also be applied here since rupture is also associated with membrane damage. However, they cannot distinguish between pore formation and rupture, seeing as the latter is a transient event. Instead, direct visualization of the bursting event can be accomplished with live-cell video

microscopy. For instance, calcein release from light-responsive polymersomes and endosomes was imaged by Vasdekis and colleagues as a burst of fluorescence towards the cytosol (Figure 4A), which is indicative of endosomal rupture rather than gradual leakage after pore formation [35]. Leakage of fluorescent dextrans after PCI treatment was visualized in real-time by De Bruin and coworkers, who noted a disappearance of the amount of labeled endosomes, indicating fast release of the compounds (Figure 4B) [34]. High-speed video acquisition was able to document an asymmetric release of tracer molecules from the endosomes, representative for a burst-like mechanism (Figure 4C). Furthermore, the authors investigated release kinetics after PCI of different pDNA-polyplexes composed of PEI, PLL and poly-D-lysine (PDL), and noticed a distinct influence of buffering on the bursting effect. Similarly, fluorescently labeled oligodeoxynucleotides (ODNs) were used as self-quenching tracer molecules for the visualization of PEI-induced endosomal rupture [66]. With a spinning disk confocal microscope, the release of ODNs was clearly visible as a burst of fluorescence filling the cytosol, followed by an accumulation of fluorescent ODNs in the nucleus (Figure 4D). These measurements are a particularly nice confirmation of the proton sponge hypothesis of buffering cationic polymers like PEI.

Though it has not been proven explicitly, one could argue that when visualizing endosomal rupture of small tracer molecules, the co-incubation of small tracer molecules might alter the actual osmotic pressure within endosomes, leading to a bursting event where there normally isn't one. An alternative rupture assay not troubled by this limitation is proposed by Maier and colleagues [67], making use of a cell line stably expressing the lectin galectin-3 (Gal-3) fused to an mCherry fluorophore. Gal-3 binds galactose residues, which under physiological conditions are present exclusively on the extracellular or intraluminal domains of membrane glycoproteins. Using live-cell video microscopy they could detect membrane rupture by viral nanoparticles in real-time based on the accumulation of cytosolic mCherry-Gal-3 on

Gewijzigde veldcode

Gewijzigde veldcode

Gewijzigde veldcode

Gewijzigde veldcode

intraluminal galactose residues in ruptured endosomal structures. Even though this assay was coined in a viral setting, the authors confirmed that this was only possible in case of fully disrupted membranes, and not in case of pore formation, extending the usefulness of this assay to all kinds of man-made nanomaterials.

3.4. Assays for studying membrane fusion

When nanomaterials are delivered by enveloped nanoparticles, e.g. liposomal formulations, endosomal escape is hypothesized to occur via fusion with the endosomal membrane. The fusion of lipid bilayers is usually assayed by a dye dilution assay, where fluorescent markers are diluted over an increased surface area (Table 2). This will result in a change in fluorescence intensity, which can be monitored with fluorescence techniques such as spectrofluorimetry or fluorescence microscopy. As a control, lipid membranes are typically lysed by a detergent for complete dilution of the fluorophores. The fluorophores used are either lipophilic in nature or coupled to lipid compounds such as phosphatidylethanolamine (PE), so that they can be efficiently incorporated in the lipid bilayer.

For example, when pyrene is loaded into a lipid membrane in a sufficiently high concentration, excitable pyrene dimers, or "excimers" will be formed. However, upon dye dilution over a larger surface area, these dimers will break apart, leading to a loss in fluorescence [59]. A more frequently used technique to monitor fluorophore dilution is Förster Resonance Energy Transfer (FRET). FRET is a distance-dependent interaction between a pair of fluorophores, a donor (D) and acceptor (A), if the emission spectrum of the donor fluorophore overlaps with the excitation spectrum of the acceptor fluorophore. If both fluorophores are in close proximity, typically 1 – 10 nm, the excited donor fluorophore can (non-radiatively) transfer its energy to the acceptor fluorophore. This results in an increase of acceptor fluorescence at the expense of donor fluorescence [44]. A frequently used FRET pair is NBD (4-chloro-7-nitrobenz-2-oxa-1,3-diazole) as a donor and rhodamine as an acceptor

Gewijzigde veldcode

Gewijzigde veldcode

dye [17, 44, 68]. Liposomal particles are double-labeled in a high concentration so that the distance between donor and acceptor allow FRET. Upon successful lipid fusion however, both fluorophores will be diluted over a larger surface area and the distance between donor and acceptor will increase, resulting in a decreased FRET efficiency. In an *ex cellulo* setting, this double-labeling can be applied to either the liposomal vector [17] or the artificial endosome [44], and FRET efficiency can be monitored by spectrofluorimetry. FRET has been used in cellular experiments as well, where the donor and acceptor fluorophores are incorporated in the lipid envelop of the nanoparticulate cargo and FRET efficiency is monitored by live cell spectral imaging microscopy [68]. A third alternative for dye dilution relies on the self-quenching characteristics of specific fluorophores when they are loaded above a certain concentration in a lipid membrane. Upon fusion, the fluorophores are diluted below their self-quenching concentration and the increase in fluorescence intensity can be monitored [55, 69-71].

Fluorophore dilution in lipid membranes is frequently used to investigate membrane fusion, either induced by CPPs [55, 59, 68], viral nanoparticles [69-71] or liposomal delivery vectors of proteins [17] or pDNA [44, 68]. Nevertheless, it should be emphasized that the major limitation of this assay is the inability to distinguish between lipid fusion and lipid mixing (Figure 5A) [72].Whereas both fusion and mixing denotes the interaction between lipid bilayers and will lead to dilution of the incorporated fluorophores over a larger surface area, lipid mixing will not result in the intended displacement of the cargo. Therefore, complementary assays have to be included to distinguish lipid mixing from lipid fusion. As an additional confirmation in an *ex cellulo* assay, it was suggested to measure the hydrodynamic size by dynamic light scattering. If fusion of lipid nanoparticles and artificial endosomes occurs, this should lead to an increase in average particle size [44]. Alternatively, content transfer from the enveloped nanoparticle has also been used to prove fusion instead of mixing

Gewijzigde veldcode
Gewijzigde veldcode
Gewijzigde veldcode
Gewijzigde veldcode
Gewijzigde veldcode
Gewijzigde veldcode
Gewijzigde veldcode
Gewijzigde veldcode
Gewijzigde veldcode
Gewijzigde veldcode
Gewijzigde veldcode
Gewijzigde veldcode
Gewijzigde veldcode
Gewijzigde veldcode
Gewijzigde veldcode

(Figure 5A). For instance, the transfer of fluorescently labeled ODNs to giant unilamellar vesicles was visualized by fluorescence microscopy [73], though this assay lacked high-throughput. Content displacement of tracer compounds has also been employed to verify lipid fusion, both towards artificial endosomes *ex cellulo* [59], and to the cytosol *in cellulo* [69]. However, such content displacement could be an indication of both membrane fusion and pore formation [72]. Therefore, both content displacement and dye dilution assays should be combined to ascertain lipid fusion. Miyauchi and coworkers proposed such a combination of dye dilution and content transfer assays, where a dual-color fluorescence labeling of an enveloped virus could distinguish lipid fusion from lipid mixing at the plasma membrane or the endosomes [69] (Figure 5B). Though this assay was used in a viral setting, the same technique could be applied to manmade enveloped nanoparticles. Basically, both the content and the envelope are labeled in fluorophores with different spectra (green and red, respectively) resulting in a yellow signal when the viral particle is intact outside of the cell or inside of the endosome. To ascertain if the particle interacts with the plasma membrane or the endosomal membrane, the dilution of the membrane dye will lead to complete loss of the red signal when infinitely diluted over the plasma membrane, or the signal will still be visible when diluted over the smaller, finite surface of the endosomes. Nevertheless, this dye dilution assay, though informative about where interaction occurs, does not distinguish lipid mixing from lipid fusion. The fluorescent content marker is incorporated to this end, as a loss of its fluorescence indicates fusion instead of mixing, regardless of the location.

Gewijzigde veldcode
Gewijzigde veldcode
Gewijzigde veldcode
Gewijzigde veldcode
Gewijzigde veldcode

3.5. Biologically relevant artificial membranes

Artificial membranes mimicking the endosomal membrane are frequently used in *ex cellulo* assays to evaluate endosomal escape in a controlled environment. The major constituents of the endosomal membrane are PC (phosphatidylcholine), PE and PS (phosphatidylserine), that are present at a ratio of 55%, 25% and 10% of total lipid content, respectively [73, 74].

Gewijzigde veldcode
Gewijzigde veldcode

Although often artificial membranes are simplified versions consisting only of PC and sometimes cholesterol, more and more studies try to mimic the endosomal membrane as accurately as possible [44]. The importance of lipid composition on membrane interactions was proven for example in a study by Berezhna and coworkers [73]. Lipid fusion was evaluated between lipoplexes and giant unilamellar vesicles (GUVs) consisting of different compositions of PC, PE, PS and sphingomyelin (SM). Remarkably, the authors find that fusion of the cationic lipoplexes with the artificial membrane and subsequent release of nucleic acids is predominantly mediated by the negatively charged PS and PE, while PC and SM are supposedly inert in this process. Similarly, a study by Yang et al. [55] showed that TAT-mediated fusion was dependent on the anionic lipid bis(monoacylglycero) phosphate (BMP), highly enriched in the intraluminal vesicles of late endosomes. Thus, these studies clearly show that the lipid composition of the artificial membrane used in the *ex cellulo* assay is of utmost importance.

Another key aspect of endosomes is the shift in pH compared to the extravesicular environment. To recreate the endosomal acidic environment, a buffer with similar pH can used to resuspend the artificial endosomes [26]. A different approach by Madani et al. involves preparing artificial large unilamellar vesicles (LUVs) with bacteriorhodopsin (BR) integrated in the lipid layer. Upon illumination, BR will act as a proton-pumping V-type ATPase, hence acidifying the LUV's interior and mimicking the late endosomal environment in a controlled manner [57].

Nevertheless, liposomes will always be a simplification of actual endosomal membranes, given the lack of proteins and lipid asymmetry [75]. In an attempt to investigate interactions with an artificial endosomal membrane with as high a biological relevance as possible, red blood cells (RBCs) have been frequently used as a model. A dye dequenching assay with RBCs as a model membrane has been used by Lakadamyali et al. [70] to study fusion in a

Gewijzigde veldcode
Gewijzigde veldcode
Gewijzigde veldcode
Gewijzigde veldcode
Gewijzigde veldcode
Gewijzigde veldcode

viral context. Similar to leakage assays, RBC integrity is frequently employed to evaluate pore formation by endosomal escape enhancing compounds, such as CPPs [26], PEI [46] or other drug delivery vectors [47, 56, 76]. Damage to the RBC membrane will lead to leakage of hemoglobin, which can be quantified by absorption measurements at 450 nm after removal of intact erythrocytes. An even more representative model membrane was used in a leakage assay by Prchla et al. [77]. HeLa cells were previously loaded with a high concentration of biotin-dextrans, after which endosomes were isolated from the cells. Afterwards, leakage of biotin-dextrans *ex cellulo* could be detected in the extravesicular environment with an ELISA assay. Interestingly, Le Blanc and coworkers adopted a similar method [71], though elaborated by incubating the pre-loaded isolated endosomes in a cytosol-mimicking solution containing buffers and ATP for continuous acidification of the purified late endosomes. Though this assay was used in a viral setting, the mimicking of the cytosolic environment can be extrapolated for use in any *ex cellulo* assay.

Gewijzigde veldcode
Gewijzigde veldcode
Gewijzigde veldcode
Gewijzigde veldcode
Gewijzigde veldcode
Gewijzigde veldcode
Gewijzigde veldcode

4. Studying endosomal escape efficiency

Of even greater practical use than elucidating the mechanism of endosomal escape, is determining if and to which extent endosomal escape occurs. Instead of investigating the membrane integrity or fusion, these (mostly cellular) assays actually monitor the amount of cytosolic cargo. Therefore, these assays are not influenced as much by the type of delivery vector as they are by the type of cargo. In this section an overview is provided of the different methods that have been reported to determine successful cytosolic delivery of nanoparticulate cargo (Table 3).

4.1. Biological activity

When the aim is to deliver biologically active molecules, e.g. therapeutic molecules in drug delivery, successful cytosolic delivery can be easily assessed by the biological activity. For

instance in case of gene therapy, a model mRNA or pDNA is used encoding for a reporter protein such as luciferase [46] or eGFP [78]. The extent of reporter protein expression is then a measure for successful delivery to the cytosol for mRNA and further to the nucleus in the case of pDNA, which only could have happened if endosomal escape has occurred. For siRNA, a mutant cell line can be used that (stably) expresses a reporter protein. The extent to which the delivered siRNA silences the reporter protein expression is then again a measure for successful cytosolic delivery of siRNA [79]. Alternatively, knockdown of a housekeeping gene can be quantified by RT-PCR [80]. For protein delivery, one can make use of model enzymes, such as the β-galactosidase enzyme, whose biological activity can be measured as the intensity of blue color after cleavage of X-Gal substrate [81]. When dealing with antigen delivery, the unique properties of APCs allow different antigen presentation assays as biological read-out. When using ovalbumin (OVA) as a model antigenic protein, the extent of OVA-delivery to APCs can be related to either the proliferation of and IL-2 secretion by OVA-peptide specific CD8+ T-cells [17], or to the amount of MHC-I dependent SIINFEKL presentation by APCs as measured by immunohistochemical analysis [35].

Gewijzigde veldcode
Gewijzigde veldcode
Gewijzigde veldcode
Gewijzigde veldcode
Gewijzigde veldcode
Gewijzigde veldcode
Gewijzigde veldcode

It is clear that the nanomaterials investigated with these assays should consist of cargo with biological activity (such as pDNA, siRNA or proteins), regardless of whether this cargo is delivered by liposomes [17], polymersomes [35] or cationic polymers such as PEI [46] or chitosan [78]. It must be noted however that the biological activity is usually the end-point of an intracellular cascade, from which endosomal escape is only one aspect. Nanoparticle uptake, dissociation of the cargo from its carrier, cytosolic translocation to the nucleus (for pDNA), transcription, translation, etc. can all influence the final outcome. Therefore, the biological assays are only an indirect measure for endosomal escape, warranting the use of other more specific assays, as described further on.

Gewijzigde veldcode
Gewijzigde veldcode
Gewijzigde veldcode
Gewijzigde veldcode

4.2. Cellular fractionation

To distinguish nanoparticulate cargo in the cytosol from that sequestered in the endolysosomal compartment, a frequently used assay involves fractionation of the cells and measuring the cargo in the cytosolic and endosomal fractions with *in vitro* assays. For example, the amount of nucleic acids [82, 83] in cytosol and endosomes was quantified with quantitative PCR after fractionation. To measure the amount of biologically active siRNA in the cytosol, the Ago-protein of the RISC-complex was immunoprecipitated from tissue lysates, followed by stem-loop PCR quantification of the amount of target siRNA present in the RISC-complex [84]. Instead of PCR quantification, it is also possible to use fluorescently labeled cargo and quantify the fluorescence in different cellular fractions/compartments. For example, fluorescently labeled dextrans and PEG-particles have been quantified this way after cellular fractionation [85]. Radio-active labeling has been used for both pDNA [50] and proteins [86] as well. It was even shown that radio-active labeled proteins can be quantified in cellular fractions from tissue lysates after *in vivo* administration [86].

We would like to highlight that for investigating endosomal escape, cellular fractionation is merely a means of distinguishing cytosolic from endosomal cargo, and should always be complemented with *in vitro* assays to measure to amount of cargo in each fraction. Though the nanomaterials which can be investigated by this endosomal escape assay are therefore only limited to whether the cargo can be measured or not, typical concerns about cellular fractionation are the labor-intensiveness of the assay, as well as the uncertainty of collecting all the fractions whilst avoiding contamination from the endolysosomal fraction in the cytosolic fraction [83]. Also, questions have been raised about the fractionation process, where uptake of macromolecules or nanomaterials might alter the vesicle buoyant density and therefore necessitate an adapted purification protocol for each nanoparticle [85]. Therefore it

Gewijzigde veldcode
Gewijzigde veldcode
Gewijzigde veldcode
Gewijzigde veldcode
Gewijzigde veldcode
Gewijzigde veldcode
Gewijzigde veldcode
Gewijzigde veldcode

seems advisable to confirm findings by the cellular fractionation assay with other assays, as the ones described below.

4.3. Fluorescence microscopy

Since most nanoparticles for intracellular delivery can be fluorescently labeled, or in some cases have intrinsic fluorescent properties, the most frequently used technique for discriminating cytosolic from endosomal cargo is via fluorescence microscopy. Given that the cargo is small enough so it can diffuse throughout the cytosol, a diffuse or punctate IFP can be related to the efficiency of endosomal escape (cfr. §3.2). This has been used to assess endosomal escape of peptides [53, 65], siRNA [87], Qdots [8] and smaller proteins [47, 88]. In most studies, the diffuse or punctate fluorescence pattern is scored visually, so that these experiments remain rather qualitative [53, 65, 81]. Yet, in some studies it was attempted to quantify the IFP. For example, the median fluorescence value of complete confocal images was proposed as a simple parameter to distinguish a punctate pattern from a diffuse intracellular distribution [88]. Alternatively, the average fluorescence intensity in regions of interest belonging to the diffuse and punctate staining can be quantified and compared [47, 87].

Fluorescent probes have also been used in a different approach to sense a change in the nanoparticle microenvironment. For example, by attaching a quencher via a disulfide bond to fluorescently tagged proteins, transfer to the cytosol of these proteins triggered an increase in fluorescence due to reduction of the disulfide bonds by cytosolic glutathione and release of this quencher [89]. Otherwise, the change in microenvironment pH between acidic endosomes and cytosol has been sensed by using fluorophores with a pH-dependent fluorescence emission [71, 90]. These fluorophores can be either attached to the nanoparticle, or be used as a nanosensor itself. To increase sensitivity to a broader pH range, these sensors are made of a pH-independent reference fluorophore and one [26, 51, 91] or two [92] dyes whose emissions

Gewijzigde veldcode
Gewijzigde veldcode
Gewijzigde veldcode
Gewijzigde veldcode
Gewijzigde veldcode
Gewijzigde veldcode
Gewijzigde veldcode
Gewijzigde veldcode
Gewijzigde veldcode
Gewijzigde veldcode
Gewijzigde veldcode
Gewijzigde veldcode
Gewijzigde veldcode
Gewijzigde veldcode
Gewijzigde veldcode
Gewijzigde veldcode
Gewijzigde veldcode

are affected differently by the pH. These ratiometric fluorescent sensors have been employed on several occasions, and more specifically to investigate the endosomal escape of proton sponge-based PEI-delivery vectors [51, 91, 92]. Nevertheless, when using such nanosensors, it should be noted that a standard curve is always required to relate fluorescence emission ratio to pH (Figure 6A). The pH obtained by these nanosensors can then be visualized in the acquired images by means of color-coding, as demonstrated in Figure 6B.

Endosomal escape can also be investigated by live-cell video microscopy. For instance, the transfer of small nanoparticulate cargo such as ODNs [66], ribozymes [93] and siRNA [84] towards the cytosol by PEI-mediated endosomal rupture was visualized by video microscopy as a burst of fluorescence from the endosomes to the cytosol. The release of pDNA, however, cannot be directly visualized since it has very limited mobility in the cytoplasm [34, 66]. The same also applies to aggregates of cargo delivered to the cytosol, as has been observed for Qdots delivered by lipofectamine, polymers, CPPs and physical techniques such as electroporation [9, 94]. This problem was circumvented by Rehman and colleagues, who prepared PEI-pDNA complexes containing in addition self-quenched fluorescently labeled ODNs as tracer compounds [66]. This allowed to detect bursting of endosomes by dequenching of the small ODNs, in a similar way as calcein could be used. Interestingly, in this way they could actually count the number of endosomal escape events per cell. Furthermore, by visualizing the rate of ODN accumulation in the nucleus (Figure 4D), they could confirm that PEI induces sudden endosomal bursting and immediate release of cargo in the cytosol, while a more gradual leakage of ODNs was observed when lipid carriers were used. Likewise, Remaut et al. made use of FRET-ODNs that could estimate both the cytosolic delivery of the ODNs based on the nuclear accumulation, and the integrity of the delivered ODNs based on the FRET signal [95]. It was found that the composition of the poly-beta-

Gewijzigde veldcode
Gewijzigde veldcode
Gewijzigde veldcode
Gewijzigde veldcode
Gewijzigde veldcode
Gewijzigde veldcode
Gewijzigde veldcode
Gewijzigde veldcode
Gewijzigde veldcode
Gewijzigde veldcode

aminoester carrier can greatly influence the amount and integrity of ODN's that are delivered to the cytosol.

Dual-color fluorescence microscopy and colocalization analysis is widely used to distinguish cytosolic nanoparticles from those that are still sequestered in the endolysosomal compartments, especially those too large to diffuse throughout the cytosol, such as pDNA polyplexes and lipoplexes. Often, (the lack of) colocalization between nanoparticles and endosomes is regarded as a measure for endosomal escape. Although colocalization is frequently visually scored [10, 96-98], it can be very well quantified by different approaches [99]. The most rudimentary way is to quantify colocalization on a per-pixel basis, where the percentage of overlapping pixels in both channels is taken as a measure for colocalization [79, 82]. Other frequently used parameters to quantify colocalization between pixels are the Pearson's [100] and Manders' correlation coefficient [51]. In our group, we have recently optimized a dual-color dynamic colocalization technique, which allows quantifying the amount of colocalization between two fluorescent labels based on their movement during a certain timeframe, in this case the colocalization between labeled endosomes and labeled pDNA-polyplexes [101, 102]. In theory, this method should also be capable of detecting correlated trajectories which diverge over time, as could be the case for endosomes and their released macromolecular cargo.

Given the widespread use of fluorescence microscopy and colocalization analysis for assaying endosomal escape, it is instructive to highlight some of the well-acknowledged technical challenges and limitations of the technique [103]. Firstly, due to the limited optical resolution of the microscope, care should be taken when evaluating diffuse vs. punctate staining, as out-of-focus light might falsely give the impression of a diffuse staining or apparent colocalized pixels. Furthermore, sub-resolution objects that are located closer together than the microscope's resolution will always appear to be colocalized, which can be especially

Gewijzigde veldcode
Gewijzigde veldcode
Gewijzigde veldcode
Gewijzigde veldcode
Gewijzigde veldcode
Gewijzigde veldcode
Gewijzigde veldcode
Gewijzigde veldcode
Gewijzigde veldcode

problematic in the perinuclear region that typically contains a high density of endosomes. Confocal microscopy certainly is preferred over wide field epi-fluorescence microscopy as it eliminates out-of-focus fluorescence to a large extent. However, due to a relatively low sensitivity, confocal microscopy can easily miss dim features like small endosomes and nanoparticles. This can be mitigated to some extent by using slow scanning speeds to collect more photons, if the fluorescent molecules do not bleach too quickly. Another frequently encountered problem is crosstalk of different fluorophores between detection channels which again may lead to false colocalization. This can be limited by recording each channel separately with sequential excitation of each of the different fluorophores [100], though the general guideline is to use fluorophores that have a minimal spectral overlap. Nevertheless, confocal microscopy is usually associated with poor temporal resolution and hence the need for fixation, which importantly has been shown to lead to artifacts concerning the endosomal sequestration [54, 104]. Nonetheless, fast confocal image acquisition in live cells is now made possible using spinning disk confocal microscopes equipped with the newest generation of sensitive CCD cameras, like the electron-multiplying CCDs or scientific CMOS cameras [66, 84].

Of equal importance for proper fluorescence microscopy is the choice of fluorescent endosomal markers. Dextrans [97] or transferrins [54] that are added to the cell medium are considered to be a non-specific endosome labeling method. Alternatively, one can pulse-chase lipophilic carbocyanine dyes in the plasma membrane [10] or use plasma-membrane specific dyes such as PKH67 [68], which will end up in most endocytic vesicles. On the other hand, specific labeling of lysosomes can be attained by using lysosome-specific markers such as lysosomal-associated membrane protein 1 (LAMP1), for example by immunofluorescence staining against LAMP1 [87] or transgene expression of an eGFP-LAMP1-construct [101]. Also acidotropic dyes can be used such as Lysotracker Blue [9, 93], Lysotracker Green [79,

Gewijzigde veldcode
Gewijzigde veldcode
Gewijzigde veldcode
Gewijzigde veldcode
Gewijzigde veldcode
Gewijzigde veldcode
Gewijzigde veldcode
Gewijzigde veldcode
Gewijzigde veldcode
Gewijzigde veldcode
Gewijzigde veldcode
Gewijzigde veldcode

80], Lysotracker Red [17, 96] and LysoSensor Green [100], which have been shown to label about 70% of the intracellular vesicles [82]. On a cautionary note, it is important to keep in mind that most acidotropic dyes are considered weak bases and might influence endosomal acidification after long incubation times. Therefore, it is recommended to follow the manufacturer's instructions. Furthermore, combining acidotropic dyes with "proton sponge"-nanoparticles for particle-lysosome colocalization has been shown to influence the outcome [105]. Indeed, though PEI-particles showed a lack of colocalization with an acidotropic dye, colocalization *was* in fact noticed with fluorescently labeled LAMP1. This was attributed to the fact that PEI has a buffering effect on the endolysosomes, thereby inhibiting staining by acidotropic dyes, a conclusion that is also confirmed by Mo and coworkers [98].

Regarding labeling of the nanoparticle of interest, one has the choice of either labeling the carrier molecules or the cargo. On the one hand it can be argued that it is best to label the cargo since it will typically be incorporated into the carrier and have the least influence on uptake and intracellular processing of the nanoparticle. Also, labeling the carrier might give rise to false conclusions, seeing as carrier dissociation is shown to already occur in the endosomes for PEI [66]. On the other hand, fluorescent labels are typically hydrophobic and might interact with the endosomal membrane and influence the displacement [66, 106]. A consensus on this has not been reached, however, warranting further studies on this topic.

4.4. Electron microscopy

Even though samples need to be fixed and require extensive preprocessing, transmission electron microscopy is still frequently used for assaying endosomal escape due to its unparalleled resolution. It allows to visually distinguish if the nanoparticles are located freely in the cytosol, or sequestered in membranous vesicles. For inorganic nanoparticles like Qdots [54], gold nanoparticles [107] and superparamagnetic iron oxide NP's [14, 108], labeling steps are usually not necessary (Figure 7A and C). However, organic nanoparticles cannot

Gewijzigde veldcode

always be easily distinguished from the cellular structures, though for polymeric nanoparticles, opinions vary. Bieber and coworkers did not label PEI-based delivery vectors, arguing that the electron dense PEI would give sufficient contrast in the TEM images (Figure 7B) [105]. On the other hand, osmium tetroxide is frequently used to label polymeric delivery vectors such as poly(lactic-co-glycolic acid) (PLGA) and PEI to enhance their contrast [49, 109]. Gold can also be employed as contrast agent, as used for instance by Gilleron and colleagues to visualize siRNA in the cytosol or in membranous vesicles [84] (Figure 7D).

Draw-backs of TEM include the necessity for fixation and that both sample preparation and analysis is very labor intensive. Usually, endosomal escape is scored visually by assessing if the majority of the nanoparticulate cargo resides in membranous vesicles, or freely in the cytosol [14, 49, 54, 105, 109]. Imelli and coworkers presented quantitative data on the amount of viral nanoparticles at the plasma membrane, in the cytosol and in the endosomal vesicles, based on data from 8 – 10 cells and 23 – 45 particles per cell [110]. The most advanced use of TEM in this context was arguably presented by Gilleron and colleagues who proposed a semi-automatic quantification of TEM images, by which siRNA coupled to 6 nm colloidal gold nanoparticles (siRNA-GNP's) are automatically detected in TEM images after setting a certain threshold (Figure 7D, left). Manual assignment of the particles to either the cytosolic or vesicular location was still required (Figure 7D, middle). Interestingly, to assess if endosomal escape of siRNA-GNP's occurred through a burst-like mechanism in a specific compartment or via gradual release, Gilleron and co-authors plotted the amount of particles in the cytosol over time [84]. Mathematical modeling showed that a gradual release of particles should lead to a linear trend, whereas a burst-like mechanism should give rise to a sigmoidal curve. Experimental data showed a sigmoidal curve in both cell lines, indicating a burst-like mechanism (Figure 7D, right).

Gewijzigde veldcode
Gewijzigde veldcode
Gewijzigde veldcode
Gewijzigde veldcode
Gewijzigde veldcode
Gewijzigde veldcode
Gewijzigde veldcode
Gewijzigde veldcode
Gewijzigde veldcode
Gewijzigde veldcode

4.5. Assessing the endosomal depot of non-delivered cargo

Additional verification of the efficiency of endosomal escape is assayed by checking the amount of cargo still sequestered in the endolysosomal compartments using previously discussed methods. By deliberately disrupting the remaining lysosomes and comparing the amount of cargo in the cytosol with normal circumstances, one can get an idea of the cargo which is inefficiently delivered. The techniques used for this endosomal disruption, e.g. proton sponge [50], Leu-Leu-OMe [38], PCI [12, 78], osmotic shock [28] etc. have previously been mentioned and the reader is referred to this section for more detail (see section 2).

Gewijzigde veldcode
Gewijzigde veldcode
Gewijzigde veldcode
Gewijzigde veldcode
Gewijzigde veldcode

4.6. Computational modeling of endosomal escape

Experimental results from different assays are frequently combined in a mathematical model in order to estimate those parameters that are difficult to measure directly. For example, computational modeling allowed Vargas et al. [111] to estimate cell binding, uptake, endosomal escape, vector unpackaging and nuclear import by combining quantitative experimental results on vector uptake, amount of pDNA in the nucleus and transfection efficiency. Similarly, Moore and colleagues [26] were able to determine the endosomal escape rate constant (k_escape) by fitting a mathematical model to experimental data obtained by ratiometric nanosensors measuring the intracellular pH with fluorescence microscopy. A study by Dinh and coworkers [112] further emphasizes the importance and usefulness of mathematical modeling, but also highlight the limitation that most mathematical models approach cellular transport mechanisms by first-order kinetics between well-defined compartments only. According to the authors, their study improves on previous mathematical models by incorporating the spatial structure of the cell, as well as taking into account the continuous movement of nanoparticles based on single-particle tracking experiments. Alternatively, computational models have been used as so-called “computational microscopy”, demonstrated by Tian et al. [113]. By coarse-grain molecular dynamics

Gewijzigde veldcode
Gewijzigde veldcode
Gewijzigde veldcode

modeling in the MARTINI force field, the authors investigate the mechanism of endosomal escape of pH-responsive dendrimers. By computational modeling, the authors could obtain a high-resolution simulation of how the endosomal membrane is destabilized by the protonated dendrimers.

5. Conclusions and future perspectives

Nanomaterials for intracellular drug delivery or cell imaging applications require an efficient cytosolic delivery mechanism. Up until now, the escape from endosomal sequestration and subsequent degradation remains a major bottleneck. In order to design improved nanomaterials, reliable assays for detecting and quantifying endosomal escape are necessary. In this review we have given an overview of assays that are currently available. Given the strengths and weaknesses of each approach, a combination of complementary methods is preferred, depending on which aspect of endosomal escape is investigated.

Not only the mechanism or the efficiency of endosomal escape is of importance. It would be of interest in future studies to try and relate endosomal escape to the time and location at which it happens in the cell. Such information could be relevant for avoiding premature degradation by the acidic environment of the late endosomes or the harsh hydrolytic conditions of the lysosomes. It is therefore expected that live cell imaging will only gain in importance. A current limitation, however, is that this is mostly based on fluorescently labeled cargo or carrier materials. As it may be that this influences the intracellular processing mechanisms or kinetics, it is of special interest to look into the capabilities of label-free microscopy techniques, such as Raman imaging, to follow up on endosomal escape.

6. Acknowledgements

Financial support by the Ghent University Special Research Fund and the Fund for Scientific Research Flanders (FWO, Belgium) is acknowledged with gratitude. KR is a post-doctoral fellow of the FWO. The authors have no other relevant affiliations or financial involvement with any organization or entity with a financial interest in or financial conflict with the subject matter or materials discussed in the manuscript apart from those disclosed. No writing assistance was utilized in the production of this manuscript.

7. References

[1] L. Rajendran, H.J. Knolker, K. Simons, Nature reviews. Drug discovery, 9 (2010) 29-42.
[2] J.G. Huang, T. Leshuk, F.X. Gu, Nano Today, 6 (2011) 478-492.
[3] S.J. Soenen, P. Rivera-Gil, J.M. Montenegro, W.J. Parak, S.C. De Smedt, K. Braeckmans, Nano Today, 6 (2011) 446-465.
[4] L.Y. Chou, K. Ming, W.C. Chan, Chemical Society reviews, 40 (2011) 233-245.
[5] D. Vercauteren, J. Rejman, T.F. Martens, J. Demeester, S.C. De Smedt, K. Braeckmans, J Control Release, 161 (2012) 566-581.
[6] N.M. Zaki, N. Tirelli, Expert Opin Drug Deliv, 7 (2010) 895-913.
[7] J.A. Mindell, Annual review of physiology, 74 (2012) 69-86.
[8] J.B. Delehanty, H. Mattoussi, I.L. Medintz, Anal Bioanal Chem, 393 (2009) 1091-1105.
[9] A.M. Derfus, W.C.W. Chan, S.N. Bhatia, Advanced materials, 16 (2004) 961-966.
[10] A.R. Bayles, H.S. Chahal, D.S. Chahal, C.P. Goldbeck, B.E. Cohen, B.A. Helms, Nano Lett, 10 (2010) 4086-4092.
[11] F. Joris, B.B. Manshian, K. Peynshaert, S.C. De Smedt, K. Braeckmans, S.J. Soenen, Chemical Society reviews, 42 (2013) 8339-8359.
[12] E. Gianolio, F. Arena, G.J. Strijkers, K. Nicolay, A. Hogset, S. Aime, Magn Reson Med, 65 (2011) 212-219.
[13] H.B. Na, I.C. Song, T. Hyeon, Advanced materials, 21 (2009) 2133-2148.
[14] S.H. Bakhru, E. Altiok, C. Highley, D. Delubac, J. Suhan, T.K. Hitchens, C. Ho, S. Zappe, Int J Nanomedicine, 7 (2012) 4613-4623.
[15] T.G. Iversen, T. Skotland, K. Sandvig, Nano Today, 6 (2011) 176-185.
[16] J. Nguyen, F.C. Szoka, Accounts of chemical research, (2012).
[17] E. Yuba, C. Kojima, A. Harada, Tana, S. Watarai, K. Kono, Biomaterials, 31 (2010) 943-951.
[18] A.K. Varkouhi, M. Scholte, G. Storm, H.J. Haisma, J Control Release, 151 (2011) 220-228.
[19] M.S. Shim, Y.J. Kwon, Adv Drug Deliv Rev, (2012).
[20] C. Pichon, L. Billiet, P. Midoux, Current opinion in biotechnology, 21 (2010) 640-645.
[21] Y.W. Cho, J.D. Kim, K. Park, The Journal of pharmacy and pharmacology, 55 (2003) 721-734.
[22] D.S. Dimitrov, Nature reviews. Microbiology, 2 (2004) 109-122.
[23] K.L. Douglas, Biotechnology progress, 24 (2008) 871-883.
[24] D. Hoekstra, J. Rejman, L. Wasungu, F. Shi, I. Zuhorn, Biochemical Society transactions, 35 (2007) 68-71.
[25] L. Wasungu, D. Hoekstra, J Control Release, 116 (2006) 255-264.
[26] N.M. Moore, C.L. Sheppard, T.R. Barbour, S.E. Sakiyama-Elbert, The journal of gene medicine, 10 (2008) 1134-1149.
[27] W. Li, F. Nicol, F.C. Szoka, Jr., Adv Drug Deliv Rev, 56 (2004) 967-985.
[28] I.S. Zuhorn, U. Bakowsky, E. Polushkin, W.H. Visser, M.C. Stuart, J.B. Engberts, D. Hoekstra, Mol Ther, 11 (2005) 801-810.
[29] J.P. Behr, Chimia, 51 (1997) 34-36.
[30] A.R. Graves, P.K. Curran, C.L. Smith, J.A. Mindell, Nature, 453 (2008) 788-792.
[31] O. Boussif, F. Lezoualc'h, M.A. Zanta, M.D. Mergny, D. Scherman, B. Demeneix, J.P. Behr, P Natl Acad Sci USA, 92 (1995) 7297-7301.
[32] C. Lin, Z.Y. Zhong, M.C. Lok, X.L. Jiang, W.E. Hennink, J. Feijen, J.F.J. Engbersen, Bioconjugate Chem, 18 (2007) 138-145.
[33] P.K. Selbo, A. Weyergang, A. Hogset, O.J. Norum, M.B. Berstad, M. Vikdal, K. Berg, J Control Release, 148 (2010) 2-12.
[34] K.G. de Bruin, C. Fella, M. Ogris, E. Wagner, N. Ruthardt, C. Brauchle, J Control Release, 130 (2008) 175-182.
[35] A.E. Vasdekis, E.A. Scott, C.P. O'Neil, D. Psaltis, J.A. Hubbell, ACS Nano, 6 (2012) 7850-7857.
[36] H. Kim, W.J. Kim, Small, 10 (2014) 117-126.
[37] Z. Qin, J.C. Bischof, Chemical Society reviews, 41 (2012) 1191-1217.

[38] V. Hornung, F. Bauernfeind, A. Halle, E.O. Samstad, H. Kono, K.L. Rock, K.A. Fitzgerald, E. Latz, Nature immunology, 9 (2008) 847-856.
[39] S. Abes, D. Williams, P. Prevot, A. Thierry, M.J. Gait, B. Lebleu, J Control Release, 110 (2006) 595-604.
[40] S.H. Lee, S.H. Choi, S.H. Kim, T.G. Park, J Control Release, 125 (2008) 25-32.
[41] S.H. Choi, S.H. Lee, T.G. Park, Biomacromolecules, 7 (2006) 1864-1870.
[42] K. Remaut, N.N. Sanders, B.G. De Geest, K. Braeckmans, J. Demeester, S.C. De Smedt, Mat Sci Eng R, 58 (2007) 117-161.
[43] D. Pozzi, C. Marchini, F. Cardarelli, H. Amenitsch, C. Garulli, A. Bifone, G. Caracciolo, Biochimica et biophysica acta, 1818 (2012) 2335-2343.
[44] Z. Hyvonen, V. Hamalainen, M. Ruponen, B. Lucas, J. Rejman, D. Vercauteren, J. Demeester, S. De Smedt, K. Braeckmans, J Control Release, 162 (2012) 167-175.
[45] S. Kakimoto, T. Hamada, Y. Komatsu, M. Takagi, T. Tanabe, H. Azuma, S. Shinkai, T. Nagasaki, Biomaterials, 30 (2009) 402-408.
[46] A. Kichler, C. Leborgne, E. Coeytaux, O. Danos, The journal of gene medicine, 3 (2001) 135-144.
[47] R.A. Jones, C.Y. Cheung, F.E. Black, J.K. Zia, P.S. Stayton, A.S. Hoffman, M.R. Wilson, Biochem J, 372 (2003) 65-75.
[48] U.F. Greber, M. Willetts, P. Webster, A. Helenius, Cell, 75 (1993) 477-486.
[49] J. Panyam, W.Z. Zhou, S. Prabha, S.K. Sahoo, V. Labhasetwar, FASEB journal : official publication of the Federation of American Societies for Experimental Biology, 16 (2002) 1217-1226.
[50] M. Colin, M. Maurice, G. Trugnan, M. Kornprobst, R.P. Harbottle, A. Knight, R.G. Cooper, A.D. Miller, J. Capeau, C. Coutelle, M.C. Brahimi-Horn, Gene Ther, 7 (2000) 139-152.
[51] K.M. Fichter, N.P. Ingle, P.M. McLendon, T.M. Reineke, ACS Nano, 7 (2013) 347-364.
[52] S. Drose, K. Altendorf, The Journal of experimental biology, 200 (1997) 1-8.
[53] F. Salomone, F. Cardarelli, M. Di Luca, C. Boccardi, R. Nifosi, G. Bardi, L. Di Bari, M. Serresi, F. Beltram, J Control Release, 163 (2012) 293-303.
[54] K. Boeneman, J.B. Delehanty, J.B. Blanco-Canosa, K. Susumu, M.H. Stewart, E. Oh, A.L. Huston, G. Dawson, S. Ingale, R. Walters, M. Domowicz, J.R. Deschamps, W.R. Algar, S. Dimaggio, J. Manono, C.M. Spillmann, D. Thompson, T.L. Jennings, P.E. Dawson, I.L. Medintz, ACS Nano, 7 (2013) 3778-3796.
[55] S.T. Yang, E. Zaitseva, L.V. Chernomordik, K. Melikov, Biophys J, 99 (2010) 2525-2533.
[56] N. Mebarek, A. Aubert-Pouessel, C. Gerardin, R. Vicente, J.M. Devoisselle, S. Begu, Int J Pharm, 454 (2013) 611-620.
[57] F. Madani, R. Abdo, S. Lindberg, H. Hirose, S. Futaki, U. Langel, A. Graslund, Biochimica et biophysica acta, 1828 (2013) 1198-1204.
[58] S.M. Van Rossenberg, K.M. Sliedregt-Bol, N.J. Meeuwenoord, T.J. Van Berkel, J.H. Van Boom, G.A. Van Der Marel, E.A. Biessen, J Biol Chem, 277 (2002) 45803-45810.
[59] E. Mastrobattista, G.A. Koning, L. van Bloois, A.C.S. Filipe, W. Jiskoot, G. Storm, Journal of Biological Chemistry, 277 (2002) 27135-27143.
[60] D.K. Bonner, C. Leung, J. Chen-Liang, L. Chingozha, R. Langer, P.T. Hammond, Bioconjug Chem, 22 (2011) 1519-1525.
[61] C.M. Wiethoff, H. Wodrich, L. Gerace, G.R. Nemerow, J Virol, 79 (2005) 1992-2000.
[62] P. Seth, D.J.P. Fitzgerald, M.C. Willingham, I. Pastan, J Virol, 51 (1984) 650-655.
[63] C.L. Moyer, C.M. Wiethoff, O. Maier, J.G. Smith, G.R. Nemerow, J Virol, 85 (2011) 2631-2641.
[64] O. Maier, D.L. Galan, H. Wodrich, C.M. Wiethoff, Virology, 402 (2010) 11-19.
[65] R. Fischer, K. Kohler, M. Fotin-Mleczek, R. Brock, J Biol Chem, 279 (2004) 12625-12635.
[66] Z. ur Rehman, D. Hoekstra, I.S. Zuhorn, ACS Nano, 7 (2013) 3767-3777.
[67] O. Maier, S.A. Marvin, H. Wodrich, E.M. Campbell, C.M. Wiethoff, J Virol, 86 (2012) 10821-10828.
[68] A. El-Sayed, I.A. Khalil, K. Kogure, S. Futaki, H. Harashima, J Biol Chem, 283 (2008) 23450-23461.
[69] K. Miyauchi, Y. Kim, O. Latinovic, V. Morozov, G.B. Melikyan, Cell, 137 (2009) 433-444.

[70] M. Lakadamyali, M.J. Rust, H.P. Babcock, X. Zhuang, Proc Natl Acad Sci U S A, 100 (2003) 9280-9285.
[71] I. Le Blanc, P.P. Luyet, V. Pons, C. Ferguson, N. Emans, A. Petiot, N. Mayran, N. Demaurex, J. Faure, R. Sadoul, R.G. Parton, J. Gruenberg, Nat Cell Biol, 7 (2005) 653-664.
[72] J. Otterstrom, A.M. van Oijen, Biochemistry, 52 (2013) 1654-1668.
[73] S. Berezhna, S. Schaefer, R. Heintzmann, M. Jahnz, G. Boese, A. Deniz, P. Schwille, Biochimica et biophysica acta, 1669 (2005) 193-207.
[74] T. Kobayashi, M.H. Beuchat, J. Chevallier, A. Makino, N. Mayran, J.M. Escola, C. Lebrand, P. Cosson, T. Kobayashi, J. Gruenberg, J Biol Chem, 277 (2002) 32157-32164.
[75] M. Traikia, D.E. Warschawski, O. Lambert, J.L. Rigaud, P.F. Devaux, Biophys J, 83 (2002) 1443-1454.
[76] C.S. Lee, W. Park, S.J. Park, K. Na, Biomaterials, 34 (2013) 9227-9236.
[77] E. Prchla, C. Plank, E. Wagner, D. Blaas, R. Fuchs, The Journal of cell biology, 131 (1995) 111-123.
[78] Z. Garaiova, S.P. Strand, N.K. Reitan, S. Lelu, S.O. Storset, K. Berg, J. Malmo, O. Folasire, A. Bjorkoy, L. Davies Cde, International journal of biological macromolecules, 51 (2012) 1043-1051.
[79] T. Suma, K. Miyata, Y. Anraku, S. Watanabe, R.J. Christie, H. Takemoto, M. Shioyama, N. Gouda, T. Ishii, N. Nishiyama, K. Kataoka, ACS Nano, 6 (2012) 6693-6705.
[80] Y. Sakurai, H. Hatakeyama, Y. Sato, H. Akita, K. Takayama, S. Kobayashi, S. Futaki, H. Harashima, Biomaterials, 32 (2011) 5733-5742.
[81] K. Maier, I. Martin, E. Wagner, Mol Pharm, 9 (2012) 3560-3568.
[82] S. Hama, H. Akita, R. Ito, H. Mizuguchi, T. Hayakawa, H. Harashima, Mol Ther, 13 (2006) 786-794.
[83] H. Akita, R. Ito, I.A. Khalil, S. Futaki, H. Harashima, Mol Ther, 9 (2004) 443-451.
[84] J. Gilleron, W. Querbes, A. Zeigerer, A. Borodovsky, G. Marsico, U. Schubert, K. Manygoats, S. Seifert, C. Andree, M. Stoter, H. Epstein-Barash, L. Zhang, V. Koteliansky, K. Fitzgerald, E. Fava, M. Bickle, Y. Kalaidzidis, A. Akinc, M. Maier, M. Zerial, Nature biotechnology, 31 (2013) 638-646.
[85] M. Manunta, L. Izzo, R. Duncan, A.T. Jones, Journal of drug targeting, 15 (2007) 37-50.
[86] S.C. Richardson, N.G. Pattrick, N. Lavignac, P. Ferruti, R. Duncan, Journal of controlled release : official journal of the Controlled Release Society, 142 (2010) 78-88.
[87] G. Basha, T.I. Novobrantseva, N. Rosin, Y.Y. Tam, I.M. Hafez, M.K. Wong, T. Sugo, V.M. Ruda, J. Qin, B. Klebanov, M. Ciufolini, A. Akinc, Y.K. Tam, M.J. Hope, P.R. Cullis, Mol Ther, 19 (2011) 2186-2200.
[88] K. Mellert, M. Lamla, K. Scheffzek, R. Wittig, D. Kaufmann, Plos One, 7 (2012) e52473.
[89] Y.J. Lee, S. Datta, J.P. Pellois, J Am Chem Soc, 130 (2008) 2398-2399.
[90] S. Nechaev, C. Gao, D. Moreira, P. Swiderski, A. Jozwiak, C.M. Kowolik, J. Zhou, B. Armstrong, A. Raubitschek, J.J. Rossi, M. Kortylewski, J Control Release, 170 (2013) 307-315.
[91] A. Akinc, M. Thomas, A.M. Klibanov, R. Langer, The journal of gene medicine, 7 (2005) 657-663.
[92] R.V. Benjaminsen, M.A. Mattebjerg, J.R. Henriksen, S.M. Moghimi, T.L. Andresen, Mol Ther, 21 (2013) 149-157.
[93] T. Merdan, K. Kunath, D. Fischer, J. Kopecek, T. Kissel, Pharm Res, 19 (2002) 140-146.
[94] J.B. Delehanty, C.E. Bradburne, K. Boeneman, K. Susumu, D. Farrell, B.C. Mei, J.B. Blanco-Canosa, G. Dawson, P.E. Dawson, H. Mattoussi, I.L. Medintz, Integr Biol (Camb), 2 (2010) 265-277.
[95] K. Remaut, N. Symens, B. Lucas, J. Demeester, S.C. De Smedt, J Control Release, 144 (2010) 65-74.
[96] N.M. Zaki, A. Nasti, N. Tirelli, Macromol Biosci, 11 (2011) 1747-1760.
[97] K. Itaka, A. Harada, Y. Yamasaki, K. Nakamura, H. Kawaguchi, K. Kataoka, The journal of gene medicine, 6 (2004) 76-84.
[98] R. Mo, Q. Sun, N. Li, C. Zhang, Biomaterials, 34 (2013) 2773-2786.
[99] V. Zinchuk, O. Zinchuk, T. Okada, Acta histochemica et cytochemica, 40 (2007) 101-111.
[100] F. Cardarelli, D. Pozzi, A. Bifone, C. Marchini, G. Caracciolo, Mol Pharm, 9 (2012) 334-340.
[101] D. Vercauteren, H. Deschout, K. Remaut, J.F. Engbersen, A.T. Jones, J. Demeester, S.C. De Smedt, K. Braeckmans, ACS Nano, 5 (2011) 7874-7884.

[102] H. Deschout, T. Martens, D. Vercauteren, K. Remaut, J. Demeester, S.C. De Smedt, K. Neyts, K. Braeckmans, International journal of molecular sciences, 14 (2013) 16485-16514.
[103] S. Bolte, F.P. Cordelieres, J Microsc, 224 (2006) 213-232.
[104] B.F. Lin, D. Missirlis, D.V. Krogstad, M. Tirrell, Biochemistry, 51 (2012) 4658-4668.
[105] T. Bieber, W. Meissner, S. Kostin, A. Niemann, H.P. Elsasser, J Control Release, 82 (2002) 441-454.
[106] K. Rombouts, T.F. Martens, E. Zagato, J. Demeester, S.C. De Smedt, K. Braeckmans, K. Remaut, Mol Pharm, (2014), (dx.doi.org/10.1021/mp4003078).
[107] Z. Krpetic, P. Nativo, V. See, I.A. Prior, M. Brust, M. Volk, Nano Lett, 10 (2010) 4549-4554.
[108] R.E. Serda, A. Mack, A.L. van de Ven, S. Ferrati, K. Dunner, Jr., B. Godin, C. Chiappini, M. Landry, L. Brousseau, X. Liu, A.J. Bean, M. Ferrari, Small, 6 (2010) 2691-2700.
[109] S. Mishra, P. Webster, M.E. Davis, Eur J Cell Biol, 83 (2004) 97-111.
[110] N. Imelli, Z. Ruzsics, D. Puntener, M. Gastaldelli, U.F. Greber, Virology journal, 6 (2009) 174.
[111] C.M. Varga, N.C. Tedford, M. Thomas, A.M. Klibanov, L.G. Griffith, D.A. Lauffenburger, Gene Ther, 12 (2005) 1023-1032.
[112] A.T. Dinh, C. Pangarkar, T. Theofanous, S. Mitragotri, Biophys J, 92 (2007) 831-846.
[113] W.D. Tian, Y.Q. Ma, Soft Matter, 8 (2012) 6378-6384.

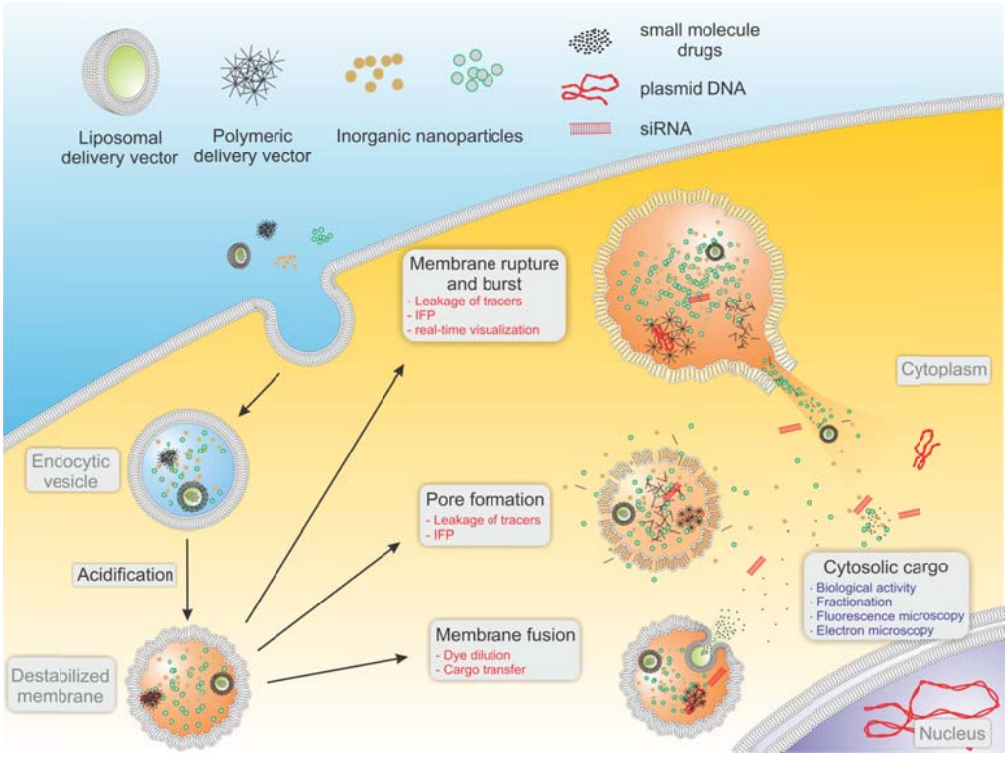
small molecule drugs
plasmid DNA
siRNA
Liposomal delivery vector
Polymeric delivery vector
Inorganic nanoparticles
Membrane rupture and burst
- Leakage of tracers
- IFP
- real-time visualization
Cytoplasm
Endocytic vesicle
Pore formation
- Leakage of tracers
- IFP
Acidification
Cytosolic cargo
· Biological activity
· Fractionation
· Fluorescence microscopy
· Electron microscopy
Membrane fusion
- Dye dilution
- Cargo transfer
Destabilized membrane
Nucleus

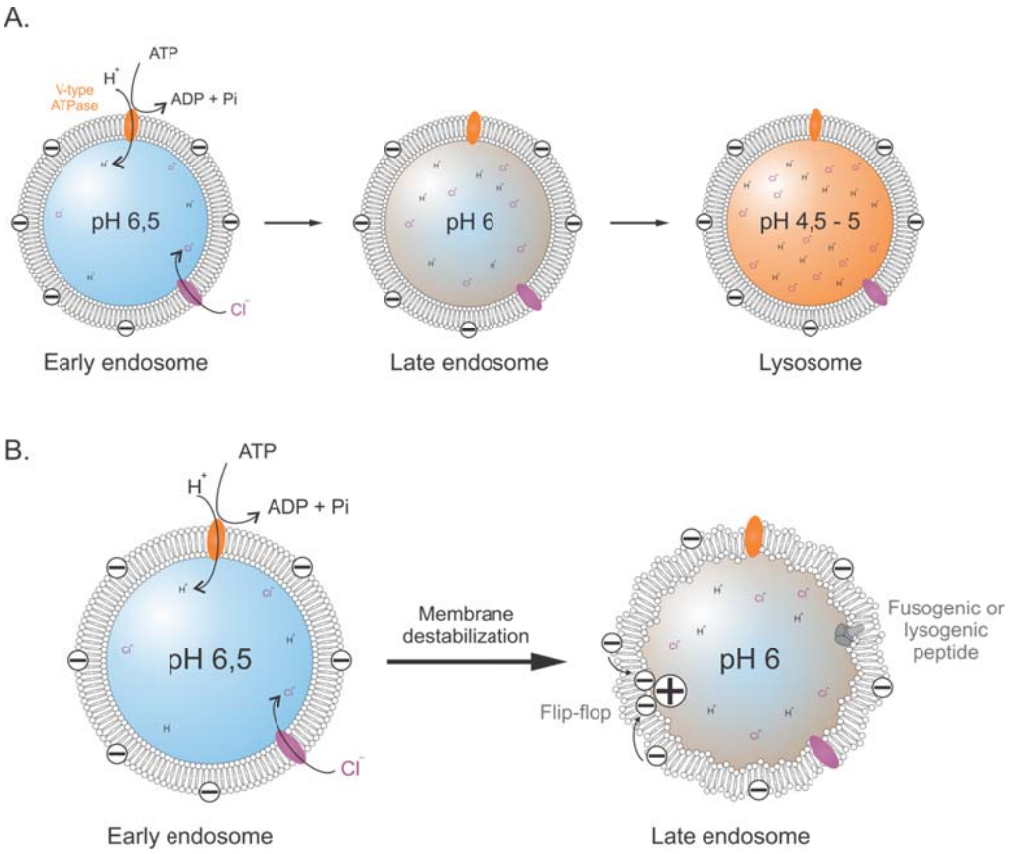
A.
ATP
H+
V-type ATPase
ADP + Pi
pH 6,5
Cl-
pH 6
pH 4,5 - 5
Early endosome
Late endosome
Lysosome
B.
ATP
H+
ADP + Pi
pH 6,5
Cl-
Membrane destabilization
pH 6
Fusogenic or lysogenic peptide
Flip-flop
Early endosome
Late endosome

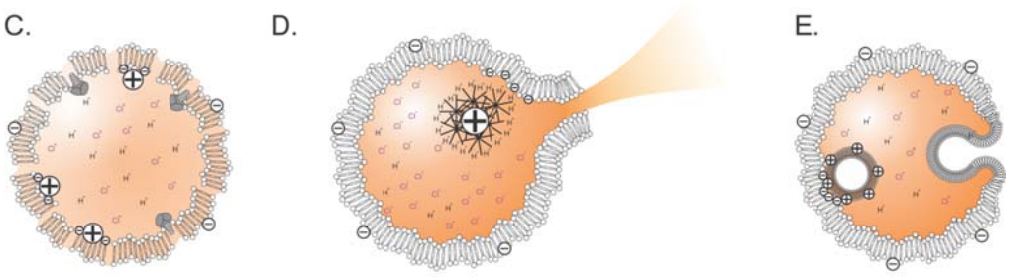
C.
D.
E.

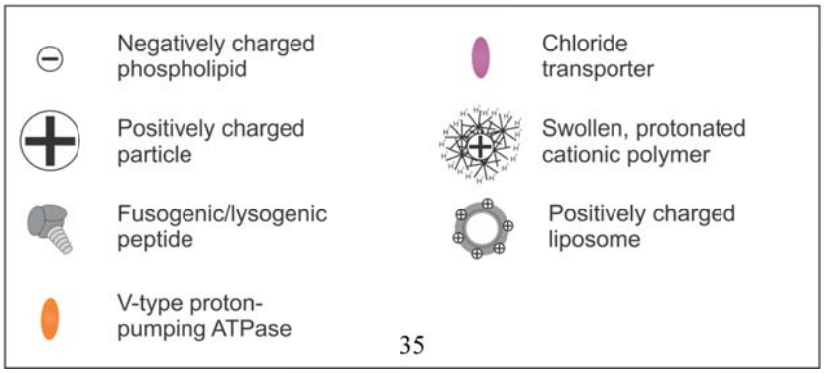
Negatively charged phospholipid
Positively charged particle
Fusogenic/lysogenic peptide
V-type proton-pumping ATPase
Chloride transporter
Swollen, protonated cationic polymer
Positively charged liposome

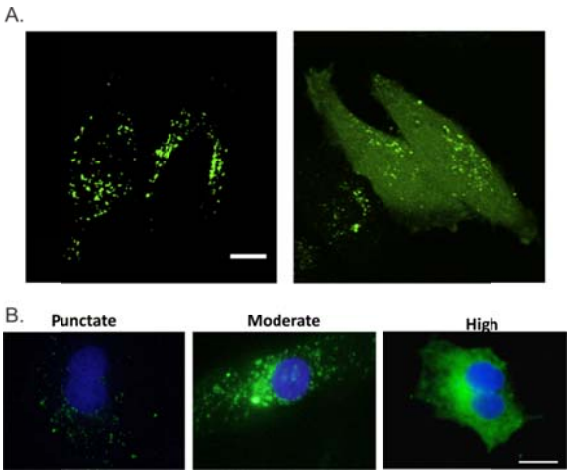
A.
B.
Punctate
Moderate
High

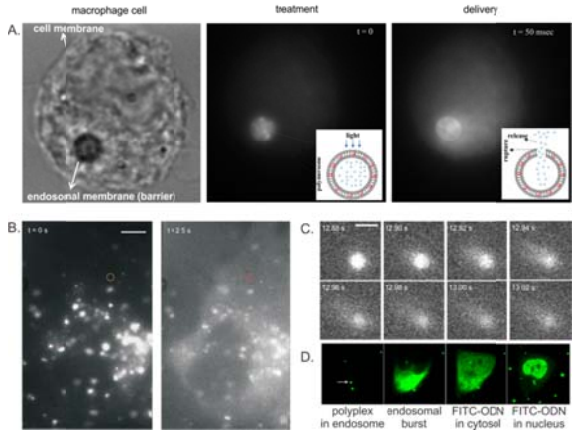
macrophage cell
treatment
delivery
A.
cell membrane
endosomal membrane (barrier)
t = 0
t = 50 msec
light
release
B.
C.
D.
polyplex in endosome
endosomal burst
FITC-ODN in cytosol
FITC-ODN in nucleus

A.

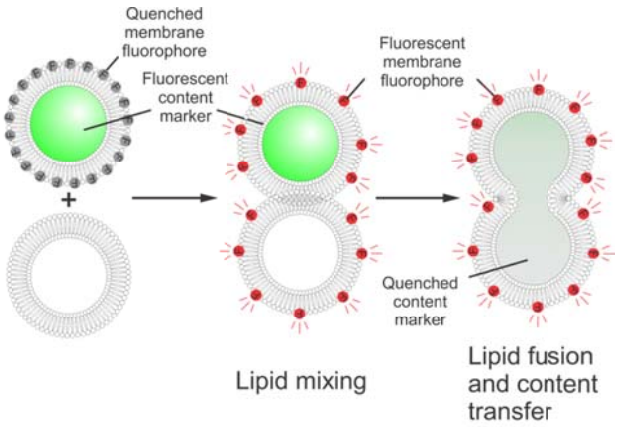

1) Membrane dye dilution	○	●	●
2) Content transfer	●	●	○
3) Combined	●	●	●

B.

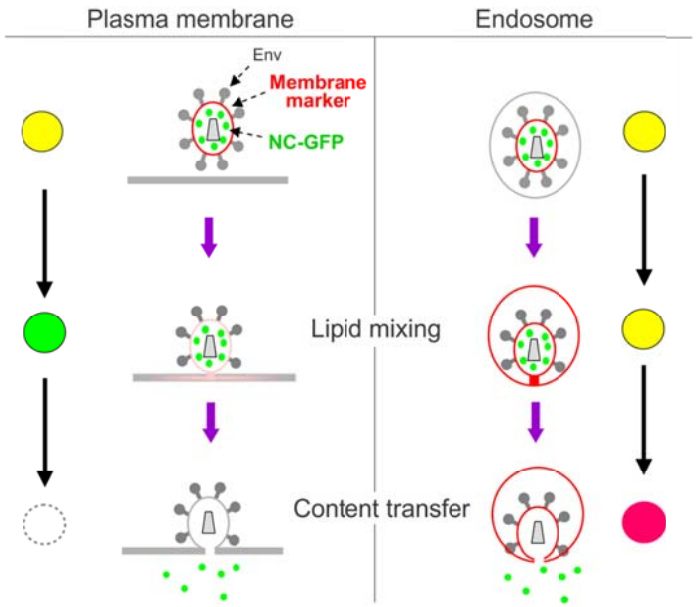

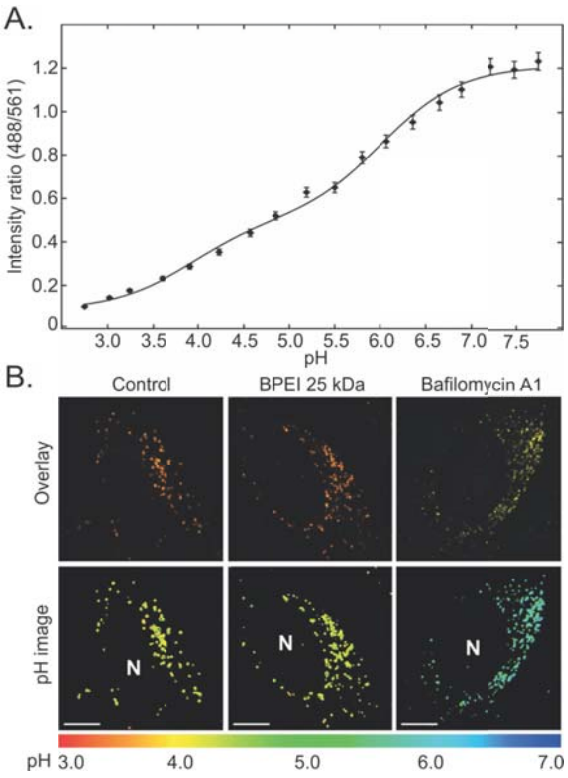
A.
Intensity ratio (488/561)
1.2
1.0
0.8
0.6
0.4
0.2
0
3.0 3.5 4.0 4.5 5.0 5.5 6.0 6.5 7.0 7.5
pH
B.
Control
BPEI 25 kDa
Bafilomycin A1
Overlay
pH image
N
N
N
pH 3.0
4.0
5.0
6.0
7.0

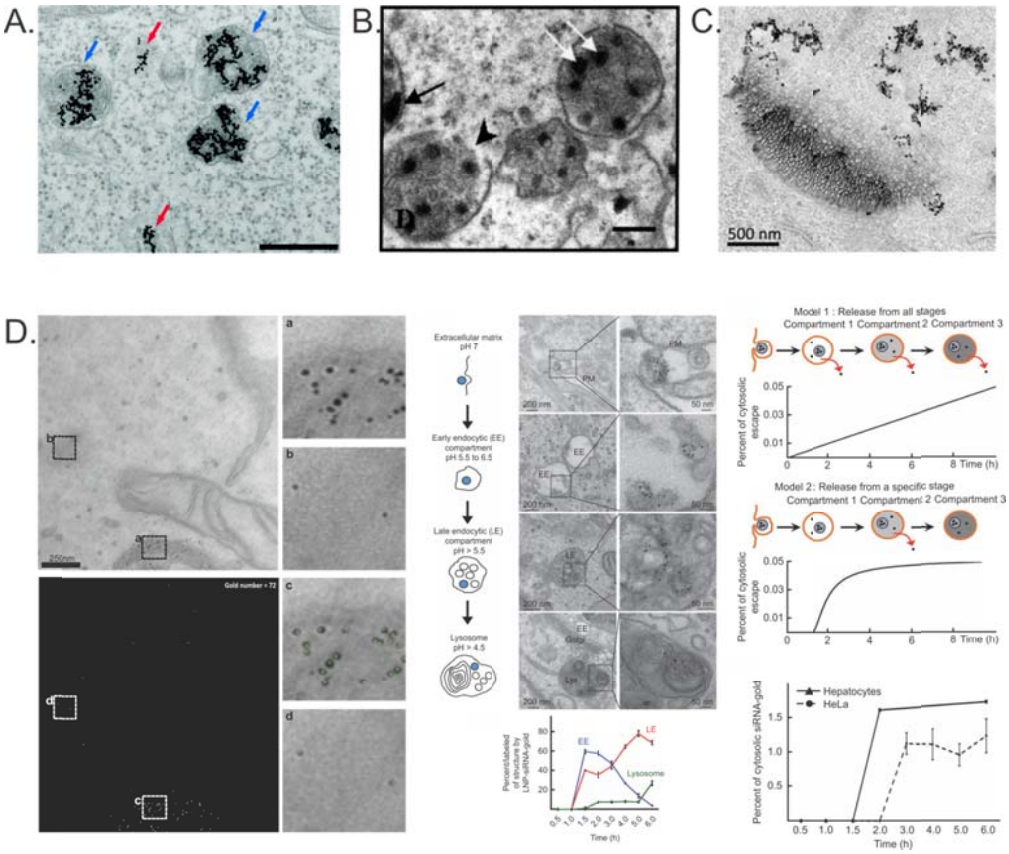
A.
B.
C.
500 nm
D.
Extracellular matrix
pH 7
Early endocytic (EE) compartment
pH 5.5 to 6.5
Late endocytic (LE) compartment
pH > 5.5
Lysosome
pH > 4.5
EE
LE
Lysosome
Time (h)
Model 1 : Release from all stages
Compartment 1 Compartment 2 Compartment 3
Model 2: Release from a specific stage
Compartment 1 Compartment 2 Compartment 3
Percent of cytosolic escape
Time (h)
Hepatocytes
HeLa
Percent of cytosolic siRNA-gold
Time (h)

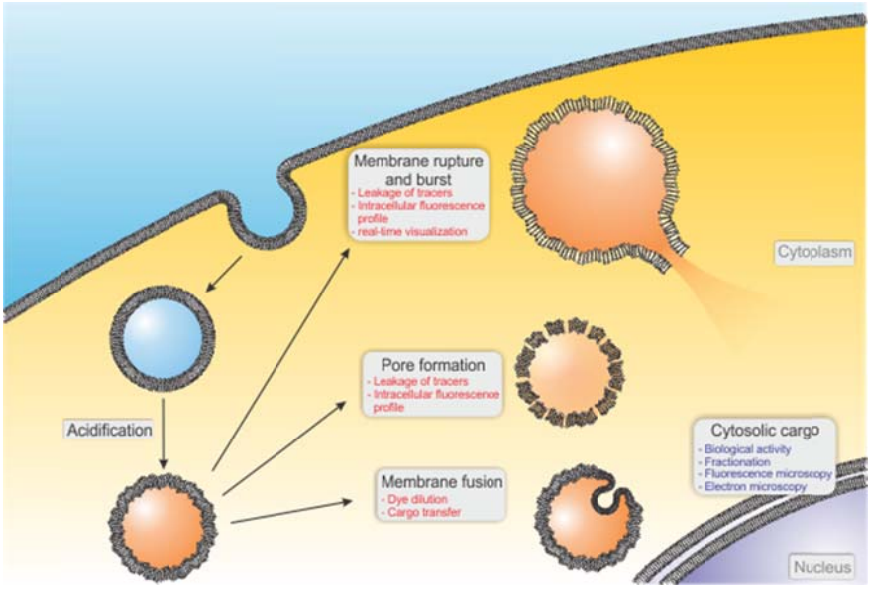
Membrane rupture and burst
- Leakage of tracers
- Intracellular fluorescence profile
- real-time visualization
Cytoplasm
Pore formation
- Leakage of tracers
- Intracellular fluorescence profile
Acidification
Cytosolic cargo
- Biological activity
- Fractionation
- Fluorescence microscopy
- Electron microscopy
Membrane fusion
- Dye dilution
- Cargo transfer
Nucleus

Figure 1: Most nanoparticles, organic and inorganic ones, for drug delivery as well as for imaging, are usually taken up by target cells via endocytosis, leading to sequestration of the cargo in the endocytic vesicles (blue interior denotes neutral pH). Acidification of the endosomes typically will trigger a destabilization of the endosomal membrane by the delivery vector (orange interior denotes acidified pH). After destabilization of the endosomal membrane, depending on the delivery vector, the cargo will be released by a bursting effect if an osmotic gradient is established by endosomal buffering, through pores formed in the endosomal membrane by persistent destabilization, or by membrane fusion if the cargo was packaged in an enveloped delivery vector. Different assays are available to investigate these endosomal escape mechanisms, as indicated in red. Also the efficiency of endosomal escape can be quantified with a variety of techniques, as indicated in blue.
IFP = intracellular fluorescence profile.

Figure 2: Different proposed mechanisms for endosomal escape. (A.) Normal acidification of the endosomes during maturation to late endosomes. ATP-driven transport of H^+-ions across the endosomal membrane by V-type ATPases produces an electrical gradient, which is balanced in part by the influx of counter-ions, presumably Cl^--ions. (B.) Upon acidification, cationic particles induce negatively charged phospholipids on the outer endosomal leaflet to flip to the luminal side of the endosome by a flip-flop effect, resulting in a charge-neutral pair and causing membrane destabilization. Alternatively, fusogenic or lysogenic peptides will undergo conformational changes in acidic environments, resulting in a triggered destabilization of the endosomal membrane. (C.) Persistent membrane destabilization by cationic nanoparticles or by fusogenic peptides can result in pore formation. (D.) When buffering compounds are found in the endolysosomal lumen, acidification will be buffered by their proton-absorbing characteristics. The increased cationic charge and swelling of the compound, as a result of the ongoing protonation of free protonable amines, will result in

membrane destabilization. A continued influx of chloride ions will create an osmotic gradient and internal pressure, leading to rupture of the endosomes and bursting of the contents into the cytosol. (E.) When an enveloped nanoparticle comes in close contact with an already destabilized membrane, e.g. by cationic charge, fusion between nanoparticle and endosomal membrane can result in cargo release in the cytosol.

Figure 3: (A.) The intracellular fluorescence profile (IFP) of 3 kDa dextrans (green fluorescence), illustrating the difference between a punctate pattern (sequestered cargo; left) and diffuse staining (cytosolic cargo; right). Scale bar 10 µm. Reprinted from [53], © 2012, with permission from Elsevier. (B.) IFP of Qdots (green fluorescence), visually classified as a punctate pattern, moderate release and a high amount of release. Blue color indicates the nucleus. Scale bar 50 µm. Reprinted with permission from [54]. © 2013 American Chemical Society.

Figure 4: Examples of the visualization of endosomal rupture by video microscopy. (A.) Light-induced release of calcein in macrophages by bursting of the endosomes, which is noticeable as a burst of calcein fluorescence in the cytosol. Reprinted with permission from [35], © 2012 American Chemical Society. (B.) A fast decrease in the amount of dextran-filled endosomes is seen, together with an increase in cytoplasmic fluorescence, indicative of endosomal bursting. Scale bar 5 µm. Reprinted with permission from [34], © 2008, with permission from Elsevier. (C) High-speed video microscopy shows the asymmetric release of dextrans from an endosome, indicative of bursting. Scale bar 2 µm. Reprinted with permission from [34], © 2008, with permission from Elsevier. (D.) Real-time visualization of endosomal escape of fluorescently labeled oligodeoxynucleotides (FITC-ODNs). A sudden release of quenched FITC-ODNs can be seen as a burst of green fluorescence, accumulating quickly in the nucleus after endosomal release. Reprinted with permission from [66], © 2013 American Chemical Society.

Figure 5: Combining membrane dye dilution and content transfer assays to verify lipid fusion. (A.) A single color membrane dye dilution assay (1) cannot distinguish between lipid mixing and lipid fusion, as the increase in red fluorescence resulting from dequenching after dye dilution could be attributed to both cases. A content transfer assay (2) can be used as a complementary assay, where fluorescence of the content marker will be lost upon dilution only after membrane fusion. Both assays can be combined when using two-color fluorescence microscopy (3), where a sub-resolution particle will appear green, yellow or red, depending on whether there is no interaction, lipid mixing or lipid membrane fusion respectively. (B.) By using two color fluorescence microscopy, Miyauchi and colleagues proposed an assay to distinguish lipid mixing from lipid fusion at the plasma membrane and in endosomes. Labeling both the envelope with a membrane marker (red fluorescent) and the core with soluble NC-GFP (green fluorescent), the viral particles outside of the cells and inside of the endosomes will emit fluorescence from both fluorophores (appearing yellow). Lipid mixing at the plasma membrane will result in almost infinite dilution of the red label and loss of the red signal. Since lipid mixing does not result in cargo displacement, the green content signal is still visible. Lipid mixing with the endosomal membrane on the other hand will still result in the presence of yellow particles in the image, as the red membrane marker will still emit fluorescence after negligible dilution in the finite endosomal membrane, and the content signal will also remain the same. When lipid fusion occurs however, either at the plasma or endosomal membrane, the content marker signal will be lost due to infinite dilution in the cell cytoplasm. Fusion at the plasma membrane, therefore, will result in loss of both signals, whereas fusion with the endosomal membrane can be ascertained by loss of green fluorescence and emission of red fluorescence from the endosomal membrane. Adapted from [69], © 2009, with permission from Elsevier.

Figure 6: (A.) Example of a standard curve obtained *in vitro*, where fluorescence emission intensity ratio is related to pH of buffers and fitted to a theoretical model. (B.) Color coded microscopic image of the intracellular pH following incubation with a three-fluorophore nanosensor. The top row shows the images as acquired by fluorescence microscopy, while the bottom row are color coded images according to the pH standard curve in A. Scale bar 10 µm. N = nucleus. Reprinted by permission from Macmillan Publishers Ltd: Molecular Therapy [92], © 2012.

Figure 7: (A.) Visualization of gold nanoparticles (GNPs) by transmission electron microscopy. Red arrows indicate cytosolic GNPs, blue arrows indicate sequestered particles. Scale bar 500 nm. Adapted with permission from [107], © 2010 American Chemical Society. (B.) Visualization of PEI-particles by TEM as electron-dense spots (white arrows). PEI-particles are seen associated with the endosomal membrane (black arrow), leading to membrane damage (arrowhead). Reprinted from [105], © 2002, with permission from Elsevier. (C.) TEM-visualization of superparamagnetic iron oxide nanoparticles. Adapted with permission from [108], © 2010 John Wiley & Sons, Inc. (D.) Quantification of endosomal escape by Gilleron and colleagues (left) Automatic detection of GNPs coupled to siRNA. (middle) A visual distinction was made between early endosomes, late endosomes and lysosomes, based on vesicular morphology. (right) Gradual release and compartment-specific release were plotted over time (respectively a linear curve and a sigmoidal curve), and experimental data was found to correlate to a compartment-specific release. Adapted by permission from Macmillan Publishers Ltd: Nature Biotechnology [84], © 2013.

- Endosomal escape is a major bottleneck in cytosolic delivery of nanomaterials
- Endosomal escape mechanisms are divided in pore formation, rupture and membrane fusion
- Several assays are used to study endosomal escape mechanisms and efficiency
- The applications and limitations of each assay should be taken into account
- Reliable quantification is necessary to enhance the endosomal escape barrier

Table 1: Overview of the different assays used to investigate pore formation by leakage of tracer compounds, with their use in cellulo or ex cellulo. Most assays are based on fluorescence, though alternatives are also listed.

	Tracer compound	Molecular Weight	Ex cellulo / In cellulo	Quenching	Measurement technique and response	reference	Comments
Tracer + quencher	ANTS	427 Da	Ex cellulo	DPX	Spectrofluorimetry Fluorescence ↑	[55]	- 2 molecules necessary
	HPTS	524 Da	Ex cellulo	DPX	Spectrofluorimetry Fluorescence ↑	[55, 56]	- 2 molecules necessary
	Fluorescein-CPP	1.500 – 3.000 Da	Ex cellulo	KI (100 mM)	Spectrofluorimetry Fluorescence ↑	[57]	- 2 molecules necessary
Self-quenching tracer	calcein	622 Da	Ex cellulo	+/- 100 mM	Spectrofluorimetry Fluorescence ↑	[58, 59]	- Quenching concentration calcein
			In cellulo	25 µM / 3,2 mM	IFP: diffuse <> punctate	[47, 60]	- Quenching concentration calcein - Quantification possible
			In cellulo	250 µM	Flow cytometry	[53]	- Quenching concentration calcein
	Sulforhodamine B	559 Da	Ex cellulo	100 mM	Spectrofluorimetry Fluorescence ↑	[61]	- Quenching concentration SulfoB
	Carboxyfluorescein	376 Da	Ex cellulo	+/- 50 mM	Spectrofluorimetry Fluorescence ↑	[45]	- Quenching concentration CF
Lysosome-specific tracer	Acridine orange	302 Da	In cellulo	Acidotropic	Flow cytometry Fluorescence ↓	[38, 47, 51]	- Measuring decrease in fluorescence - Compare to normal cells
	DQ-ovalbumin	45.000 Da	In cellulo	Before proteolytical processing	IFP: diffuse <> punctate	[38]	- Only fluorescence after lysosomal degradation
Reporter assays	Pseudomonas exotoxin	71.000 Da	In cellulo	Only active in cytosol	Protein synthesis ↓ [^{3}H]-leucine	[62]	- No hydrophobic fluorophores - Important to normalize
	α-sarcin	18.000 Da	In cellulo	Only active in cytosol	Protein synthesis ↓ [^{35}S]-methionine	[63]	- No hydrophobic fluorophores - Important to normalize
	saporin	30.000 Da	In cellulo	Only active in cytosol	Protein synthesis ↓ MTT assay	[64]	- No hydrophobic fluorophores - Important to normalize
Large tracer compounds	Protein	20.000 Da	Ex cellulo	Radio-active labeling	Gel electrophoresis and radio-activity measurement	[58]	- No hydrophobic fluorophores - Relevant for cells?

Table 2: Successful lipid-lipid fusion leads to a dilution of the incorporated fluorophores over a larger surface area. Dye dilution can be detected in a number of ways: dimer quenching, resulting in loss of fluorescence; FRET, resulting in a shift in fluorescence ratio of two fluorophores; dye dequenching, resulting in an increase in fluorescence due to dequenching of a self-quenching fluorophore.

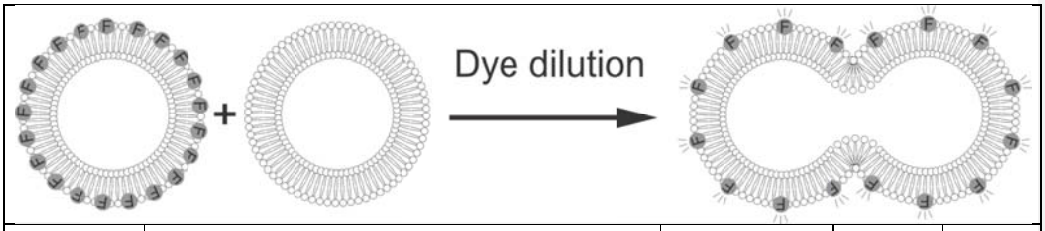

Dimer quenching	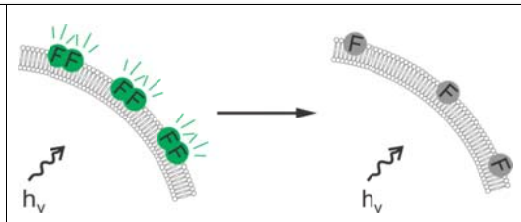	**PyrPC** λ_{exc}=345 nm; λ_{em}=480 nm	Ex cellulo	[59]
FRET	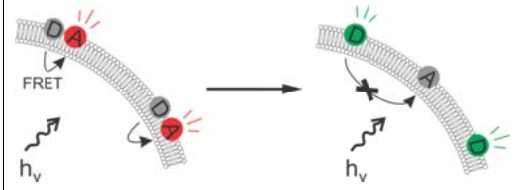	**NBD (D)** λ_{exc}=465 nm; λ_{em}=535 nm	Ex cellulo	[17, 44]
		Rhodamine (A) λ_{exc}=545 nm; λ_{em}=576 nm	In cellulo	[68]
Dye dequenching	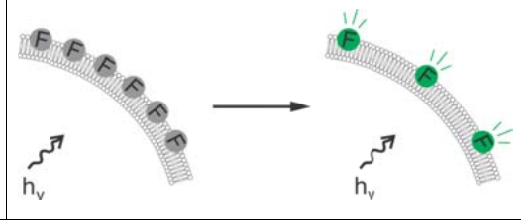	**Rhodamine** λ_{exc}=545 nm; λ_{em}=576 nm	Ex cellulo	[55]
		DiD λ_{exc}=633 nm; λ_{em}=650 nm LP	In cellulo	[69, 70]
		DiI λ_{exc}=549 nm; λ_{em}=565 nm	In cellulo	[71]

FRET: Förster resonance energy transfer; F = fluorophore; D = donor; A = acceptor; NBD = 4-chloro-7-nitrobenz-2-oxa-1,3-diazole; PE = phoshpatidylethanolamine; DiD = 1,1'-dioctadecyl-3,3,3',3'-tetramethylindodicarbocyanine; DiI = 1,1'-dioctadecyl-3,3,3',3'-tetramethylindocarbocyanine; PyrPC = 1-Hexadecanoyl-2-(1-pyrenedecanoyl)-sn-glycero-3-phosphocholine;

Table 3: Overview of different techniques used to monitor cargo displacement to the cytosol.

Distinguish cytosolic fraction from sequestered fraction	Measuring technique	Use	Reference	Pro's	Con's
Biological activity in cytosol	reverse transcriptase quantitative PCR	- Knockdown of reporter or house-keeping gene by siRNA	[80]	- *In vivo* measurements - Easy high-throughput quantification	- Indirect measure - Fixed end time-point - Limited to siRNA
	Spectro / luminometer	- Expression or knockdown of reporter gene - Enzyme activity	[46, 79] [81]	- Applicable to different cargo - Easy read-out - Easy high-throughput quantification	- Indirect measure - Population average - Fixed end time-point
	Flow cytometry	- Expression or knockdown of reporter gene	[78]	- Applicable to different cargo - Fast and easy read-out - Easy high-throughput quantification - Single-cell measurements	- Indirect measure - Fixed end time-point
	ELISA	- Detection of IL-2 secretion as antigen presentation assay	[17]	- Live-cell measurement - Easy high-throughput quantification	- Indirect measure - Limited to antigen delivery to APCs
	Immunofluorescence microscopy	- Immunostaining of SIINFEKL as antigen presentation assay	[35]	- Easy high-throughput quantification	- Indirect measure - Limited to antigen delivery to APCs - Fixed end time-point
Cellular fractionation	Quantitative PCR	- Amount of DNA	[82, 83]	- Cytosol <> endosomes - Easy high-throughput quantification - *In vivo* measurements	- Labor-intensive cellular fractionation - Carrier-bound DNA? - Fixed end time-point
	Stem-loop PCR	- Amount of biologically active siRNA bound to RISC	[84]	- Cytosol <> endosomes - Easy high-throughput quantification - *In vivo* measurements - Only active cargo	- Labor-intensive cellular fractionation - Immunoprecipitation step necessary - Fixed end time-point - Limited to siRNA
	Radio-activity	- Amount of DNA - Amount of proteins	[50] [86]	- Cytosol <> endosomes - Easy high-throughput quantification - *In vivo* measuremen	- Labor-intensive cellular fractionation

				ts	
Intracellular fluorescence profile	Wide field epi-fluorescence or confocal microscopy	- Visual scoring - Quantification	[53, 65, 81] [47, 87, 88]	- Cytosol <> endosomes - Easy read-out - Specific labeling	- Limited to small cargo - Difficult quantification - Fluorescent labeling
Fluorescent microenvironment sensors	Fluorescence microscopy	- Measure reductive environment - Measure difference in pH	[89] [26, 51, 71, 90-92]	- Easy read-out - Specific labeling - Live cells	- Indirect measure - Standard curve necessary - No quantification - Fluorescent labeling
Real-time visualization of endosomal escape	Live-cell video microscopy	- Visualize bursting of endosomes - Visualize fusion with endosomes	[66, 84, 93] [69-71]	- Cytosol <> endosomes - Mechanism of endosomal escape - Live cells - Specific labeling	- Limited to small cargo - Low throughput quantification - Fluorescent labeling
Colocalization	Confocal microscopy	- Visual scoring - Quantification	[10, 96-98] [51, 79, 82, 100]	- Cytosol <> endosomes - Easy read-out - Specific labeling - All cargo	- Difficult quantification - Fluorescent labeling - Limited temporal resolution - Fixation sometimes necessary
Visual assessment	Electron microscopy	- Visual scoring	[14, 49, 54, 84, 105, 108, 109]	- Very high resolution - Labeling not always necessary	- Fixation artifacts - Low throughput quantification